NASA Technical Memorandum 85777

NASA-TM-85777 19840014485

DEVELOPMENT AND ANALYSIS OF A STOL SUPERSONIC CRUISE FIGHTER CONCEPT

Samuel M. Dollyhigh, Willard E. Foss, Jr.,
Shelby J. Morris, Jr., Kenneth B. Walkley,
E. E. Swanson, and A. Warner Robins

FOR REFERENCE

NOT TO BE TAKEN FROM THIS ROOM

MARCH 1984

NASA

National Aeronautics and
Space Administration

Langley Research Center
Hampton, Virginia 23665

TABLE OF CONTENTS

i

SUMMARY

The application of advanced and emerging technologies to a fighter aircraft concept is presented. The concept, which is referred to as the twin-boom fighter (TBF-1), relies on a two-dimensional vectoring/reversing nozzle to provide STOL performance while also achieving efficient long range supersonic cruise. A key feature is that the propulsion package is placed so that the nozzle hinge line is near the aircraft center-of-gravity to allow large vector angles and, thus, provide large values of direct lift while minimizing the moments to be trimmed. The configuration name is derived from the long twin booms extending aft of the engine to the twin vertical tails which have a single horizontal tail mounted atop and between them. Advanced technologies utilized were an advanced engine (1985 state-of-the-art), superplastic formed/diffusion bonded titanium structure, advanced controls/avionics/displays, supersonic wing design, and conformal weapons carriage. The integration of advanced technologies into this concept indicate that large gains in takeoff and landing performance, maneuver, acceleration, supersonic cruise speed, and range can be achieved relative to current fighter concepts.

PART I. - INTRODUCTION

S. M. Dollyhigh

Increased national interest is being expressed in efficient supersonic cruise military airplanes with short takeoff and landing (STOL) performance. The National Aeronautics and Space Administration, in keeping with its charter to investigate innovative concepts with potential performance payoffs, has undertaken research related to such a STOL supersonic cruise concept. Achievement of efficient supersonic cruise in a fighter aircraft also designed for STOL capability requires careful integration of advanced technologies. Of particular importance is the manner in which the propulsion system is integrated. Conventional concepts often employ auxiliary engines to achieve STOL performance. These engines and associated ducting tend to increase fuselage cross-sectional area to the point where increases in wave drag prevent efficient supersonic cruise performance. Thrust vectoring of the primary engines can also cause problems by requiring oversized control surfaces to trim the large pitching moments associated with thrust vectoring. The Mach 2.0 fighter concept presented in this paper attempts to overcome some of these problems through innovative airframe/propulsion system integration.

The concept referred to as the twin boom fighter (TBF-1) relies on a two-dimensional vectoring/reversing nozzle to achieve STOL performance. The propulsion package is placed near the aircraft center-of-gravity to allow large thrust vector angles and thus provide large values of direct lift while minimizing thrust-induced moments which must be trimmed aerodynamically. Further, the introduction of thrust vectoring at the wing trailing edge has been shown to induce a supercirculation (or thrust induced lift) on the wing (reference I-1). Also, with the engines located forward of the wing trailing edge, the incorporation of a system for blowing along the trailing-edge control surfaces for high lift and control at low speeds will be facilitated. Low-speed control is probably the limiting factor in obtaining minimum operational field length for this type of configuration. Sufficient low-speed control may permit the removal of the thrust reverser with attendant weight and performance benefits.

Aerodynamic shaping of the twin boom fighter evolved from research on twin fuselage supersonic transport concepts (ref. I-2). Although the TBF-1 is not a pure multi-body configuration, it does reflect the earlier twin fuselage efforts.

2

It is also a highly blended concept in order to achieve the required volume and minimize drag.

The development, design, and analysis of the twin boom fighter concept are presented in this paper. The TBF-1 concept was sized for a typical supersonic mission of 500 n.mi. radius with all supersonic cruise at Mach 2.0. The most significant mission constraints and/or requirements were that the takeoff and landing ground roll not exceed 1,000 feet under standard conditions, and that the transonic acceleration and maneuver performance be comparable with existing state-of-the-art fighter aircraft. The TBF-1 configuration sized to these requirements is similar in size and weight to current transonic fighter aircraft. Details of the design development, aerodynamic design, propulsion system and integration, mass properties, sizing, and mission performance are presented. The sensitivities of takeoff and landing field length and mission performance to various parameters are also included. The configuration as reported herein is intended to serve as a baseline concept for the assessment of advanced technologies from a systems standpoint.

REFERENCES

I-1. Capone, Francis J.: A Summary of Experimental Research on Propulsive-Lift Concepts in the Langley 16-Foot Transonic Tunnel. AIAA Paper No. 75-1315, 1975.

I-2. Maglieri, Domenic J.; and Dollyhigh, Samuel M.: We Have Just Begun to Create Efficient Transport Aircraft. Astronautics and Aeronautics, February 1982, pp. 26-38.

PART II. - CONFIGURATION DESCRIPTION

E. E. Swanson

The twin boom fighter concept is a twin-engine single-pilot Mach 2.0 supersonic cruise configuration designed for a payload consisting of two short range and four long range air-to-air missiles. Figure II-1 is a general arrangement of the study concept designated TBF-1. An inboard profile is shown in figure II-2. Photographs of a display model of the configuration are shown in figures II-3 and II-4.

The wing planform is similar to an arrow wing with a trailing-edge cutout in the area occupied by the nozzles. The highly swept glove region, which constitutes the leading edge of the wing, is shaped to utilize leading-edge thrust at supersonic cruise, as well as to locate the aerodynamic center longitudinally close to the aircraft center-of-gravity and nozzle hinge line at the takeoff condition. The highly cambered wing was designed for minimum drag and favorable zero-lift pitching moment characteristics at the Mach 2.0 cruise condition. The low-speed high-lift system consists of one leading-edge flap, two trailing-edge flaps, and a flaperon. A substantial portion of the total fuel is carried in the wing as shown in figure II-2. One AIM-9L Sidewinder short range missile with its launch rail and support structure are mounted on each wing tip. The four advanced long range missiles are semi-submerged and mounted on the wing lower surface. These missiles have retracted stabilizing and maneuvering fins that are deployed upon missile release. It was assumed that each missile would have weight and performance similar to the AIM-54A Phoenix system.

The cockpit is on the aircraft centerline with the ejection seat, advanced side arm controller, and instrument pedestal similar to the F-16. Forward looking radar and associated equipment are mounted in the nose section forward of the cockpit. This nose section and the cockpit area are highly blended with the inlet and propulsion package to provide minimum frontal area. The remaining avionic, electrical, and environmental control systems are located aft of the pilot's main bulkhead. The nose landing gear has a single wheel, arrangement mounted on the forward face of the main bulkhead and retracts forward into a cavity beneath the avionics bay. The main landing gear has a single wheel, single strut arrangement mounted on each boom and retracts aft into the boom.

The two advanced technology, low-bypass-ratio turbofan engines are slightly canted and located aft of the pilot's bulkhead. A common gearbox is positioned between the engines and driven from each engine by a quill shaft. This gearbox provides power for hydraulic pumps, electric generators, engine accessories, and input from the jet fuel starter. The engine nozzles are located between the booms close to the aircraft center-of-gravity and are two-dimensional. Each nozzle is variable and vectorable and incorporates a thrust reverser to provide reduced takeoff and landing runs and to improve in-flight maneuverability. Two-dimensional external compression inlets are located on either side of the cockpit.

Twin booms are mounted at the junction of the wing and engine nacelle and extend aft to the twin vertical tails. These long booms provide volume for fuel and length to tailor the configuration for low wave drag. They also provide a substantial moment arm for the horizontal tail which is mounted atop the twin verticals. The booms have a shielding effect on the engine exhaust, and thus reduce the infrared signature. The horizontal tail is hinged so that most of the tail area can rotate for control while the rectangular center section remains fixed to provide a structural tie between the twin vertical tails.

A volume utilization diagram for the configuration is presented in figure II-5. Total aircraft volume is 1,250 ft^3, and, at a takeoff gross weight of 47,000 lbf, the overall density is 37.6 lbf/ft^3.

Additional fuel for aircraft ferry missions can be provided by either four store-cavity tanks or two fuel pallets. As shown in figure II-6, the store-cavity tanks have the same geometry as the conformally mounted stores. A fairing has been added to the base to reduce the installed drag. These tanks have a capacity of 98.5 gallons each, and can be carried at all flight speeds including cruise at Mach 2.0. The conformal fuel pallets are mounted underneath the wing in the area normally occupied by the large stores. A pair of pallets with capacities of either 450 or 600 gallons each can be used. In both instances the pallet geometries have been tailored to provide a low-drag installation for Mach numbers up to 1.4. Figure II-7 illustrates the pallet geometry, and the installed pallet is shown in figure II-8. Note that the wing volume normally occupied by the stores is also used for ferry fuel.
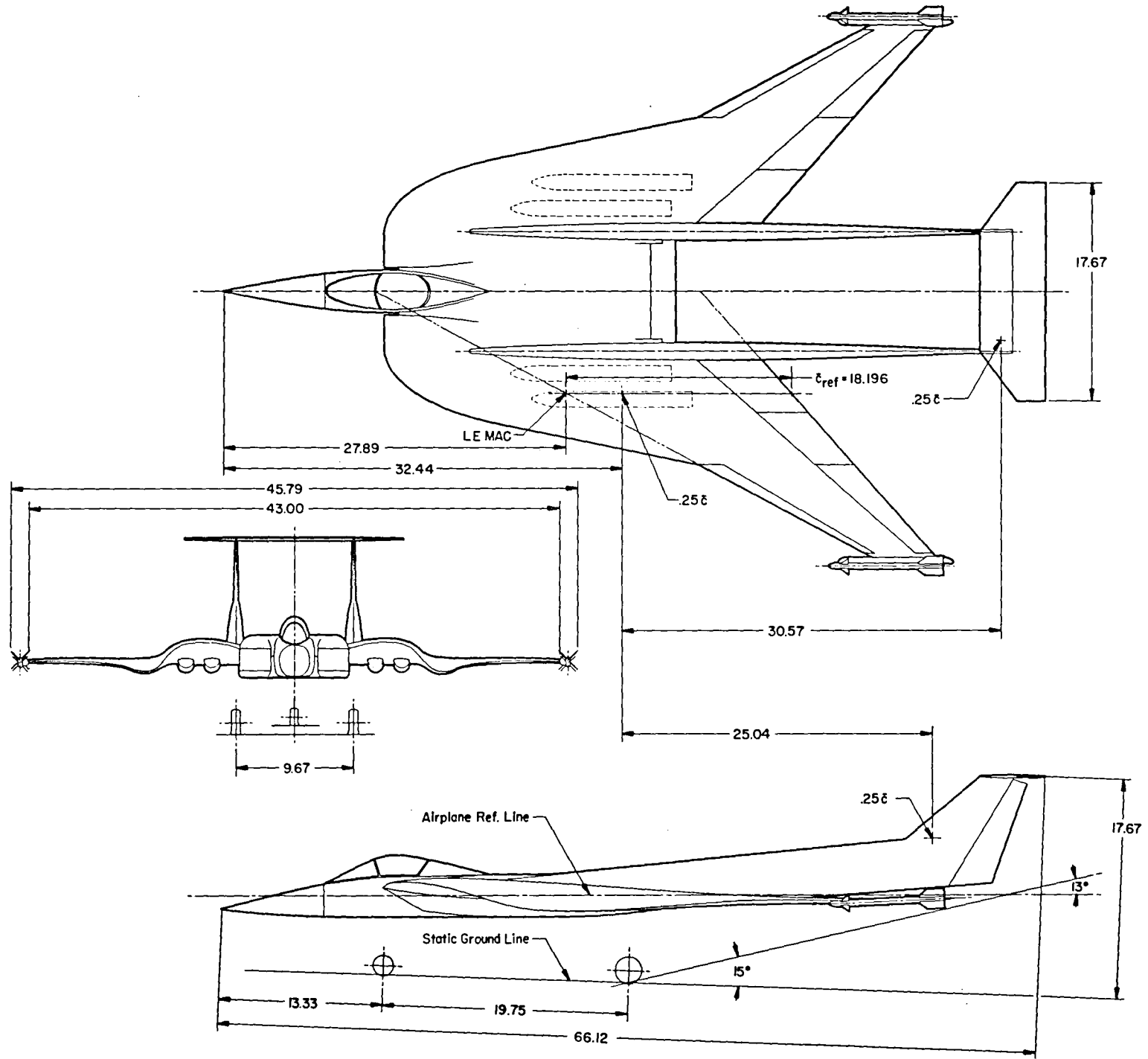
$\bar{c}_{ref} = 18.196$

.25$\bar{c}$

17.67

27.89

32.44

LE MAC

.25$\bar{c}$

45.79

43.00

30.57

9.67

25.04

.25$\bar{c}$

Airplane Ref. Line

17.67

Static Ground Line

13°

15°

13.33

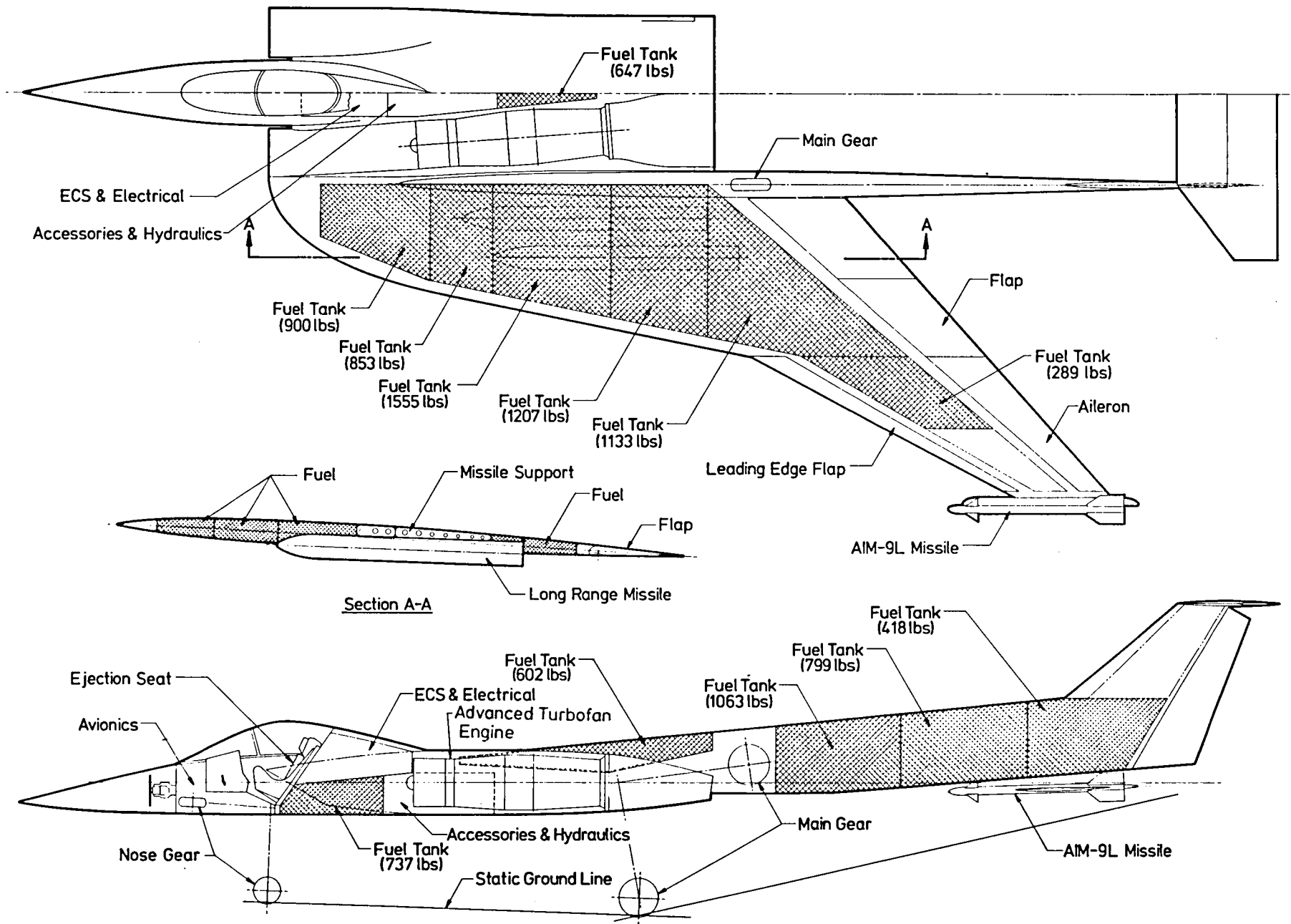19.75

66.12

Figure II-1. – General arrangement.
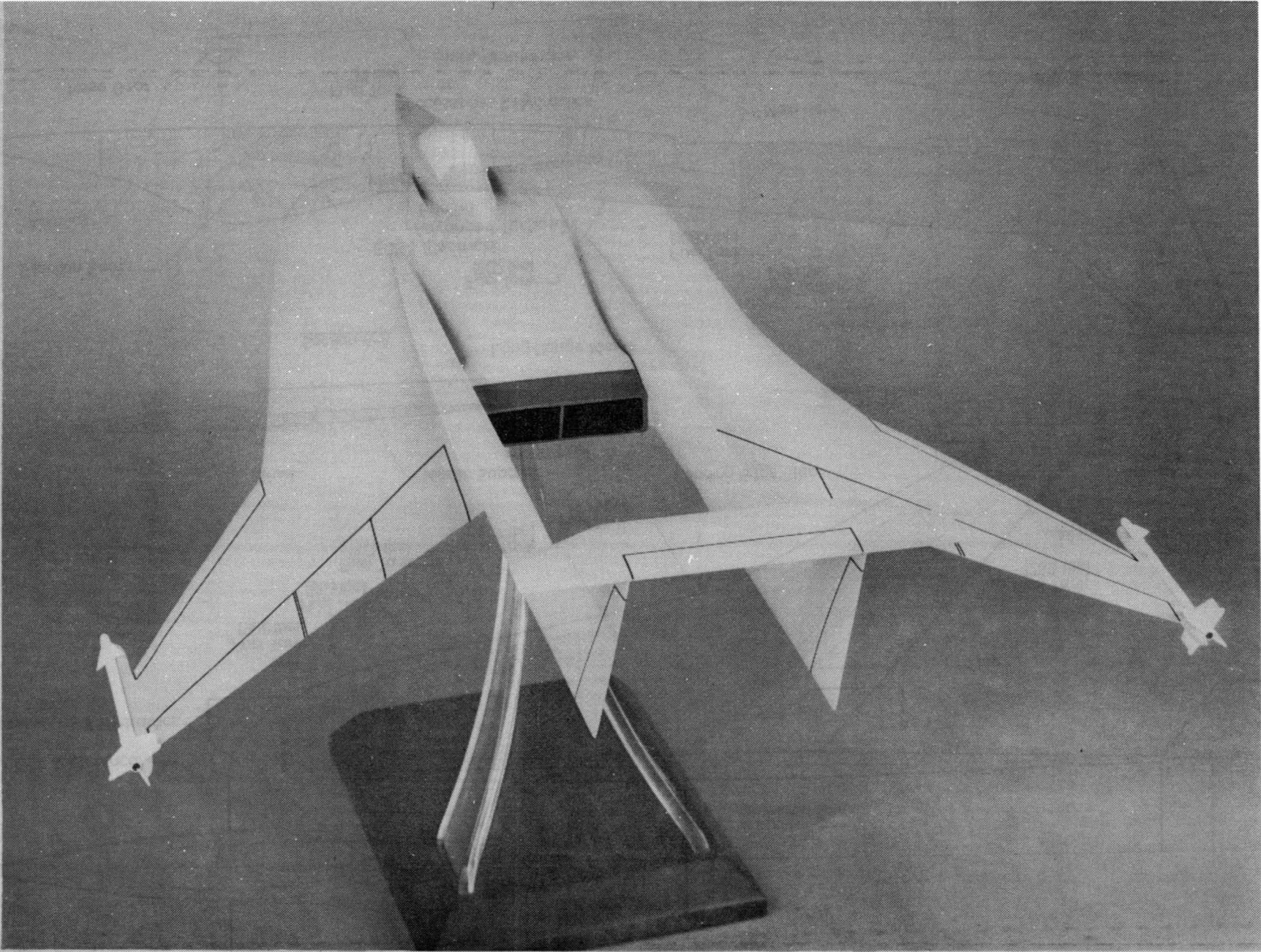
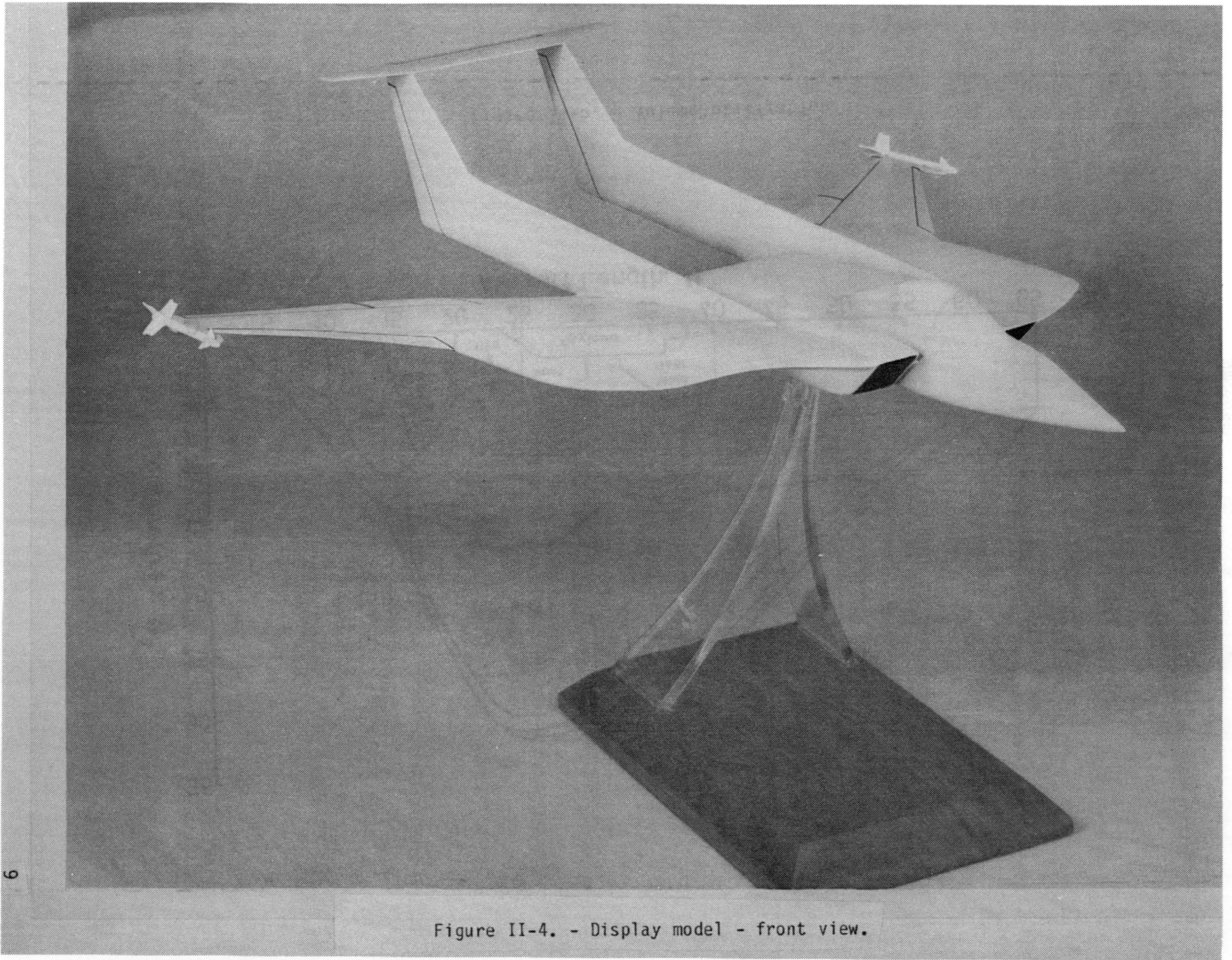Figure II-2. – Inboard profile.

Figure II-3. - Display model - rear view.
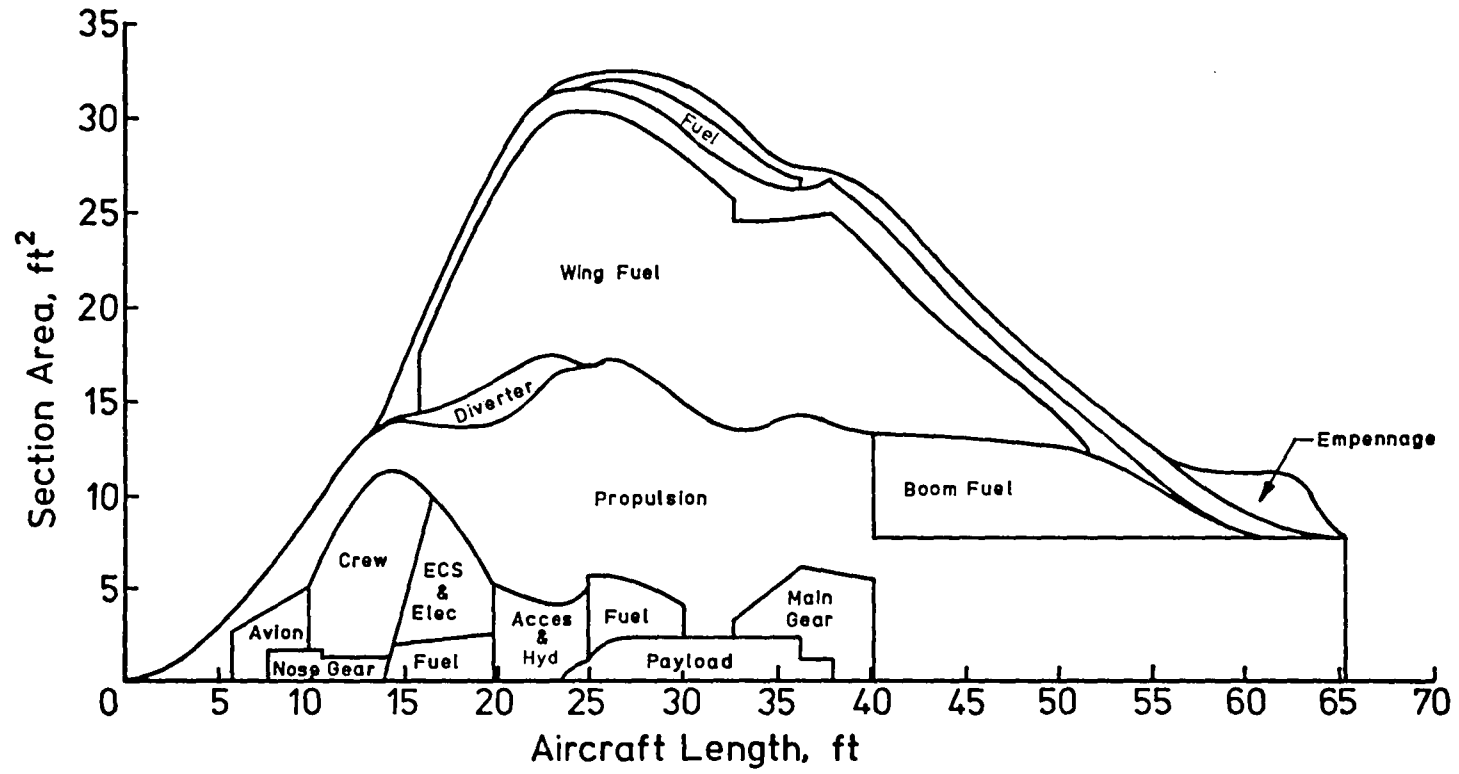
Figure II-4. - Display model - front view.

Figure II-5. - Volume utilization.
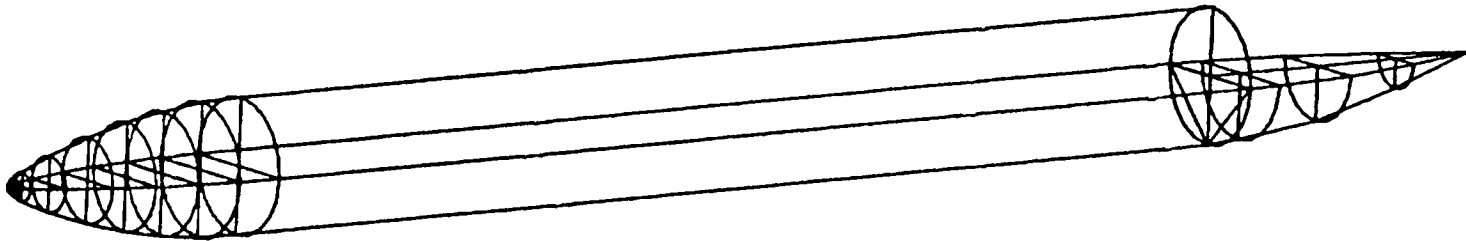
- Single tank capacity - 98.5 gallons

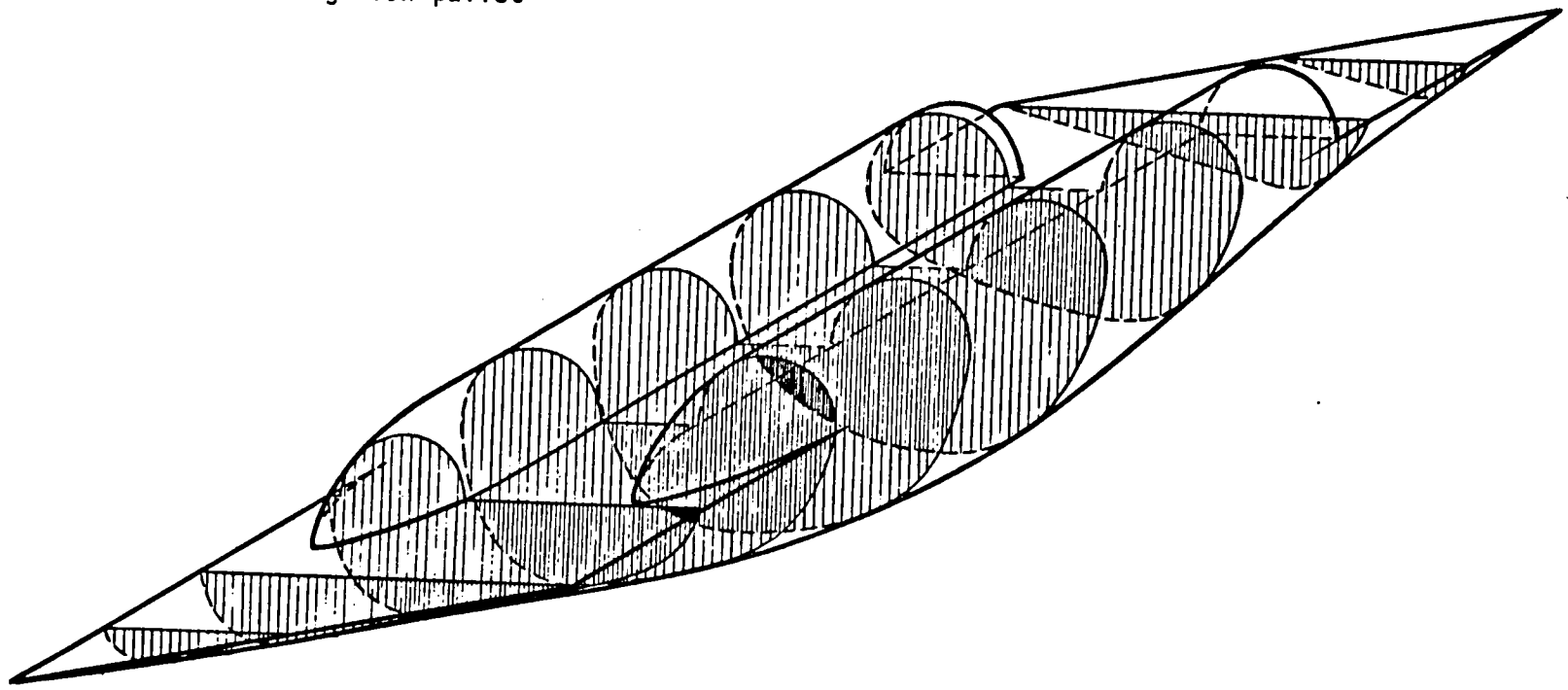Figure II-6. - Store-cavity tank.

● Left-hand side

● 450 gallon pallet
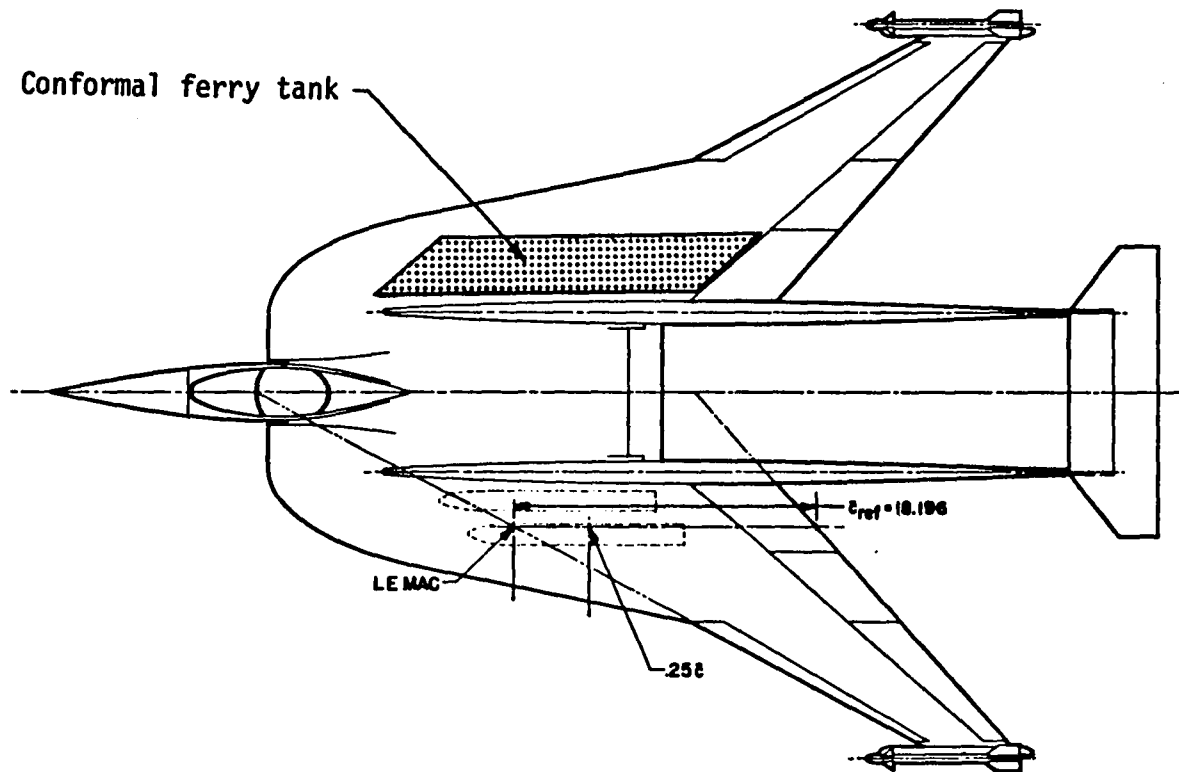

Figure II-7. - Conformal fuel pallet.

Conformal ferry tank

$c_{ref} = 18.196$

LE MAC

.25c

Figure II-8. - Conformal fuel pallet installation.

13

PART III. - PROPULSION SYSTEM ANALYSIS

S. J. Morris, Jr.

The engine selected for the study is an advanced-technology, low-bypass-ratio turbofan. This military engine is based on company-proprietary engine data and represents 1985 technology readiness. The sea-level, static, maximum augmented thrust is 31,955 pounds. The thrust-to-weight ratio, exclusive of the nozzle, is 11.5; this ratio decreases to 9.06 with the inclusion of a two-dimensional, converging-diverging nozzle for thrust vectoring and thrust reversing. The engine data incorporates MIL SPEC inlet total-pressure recovery to account for installation effects. The center of gravity (CG) and dimensions of this engine are presented in figure III-1.
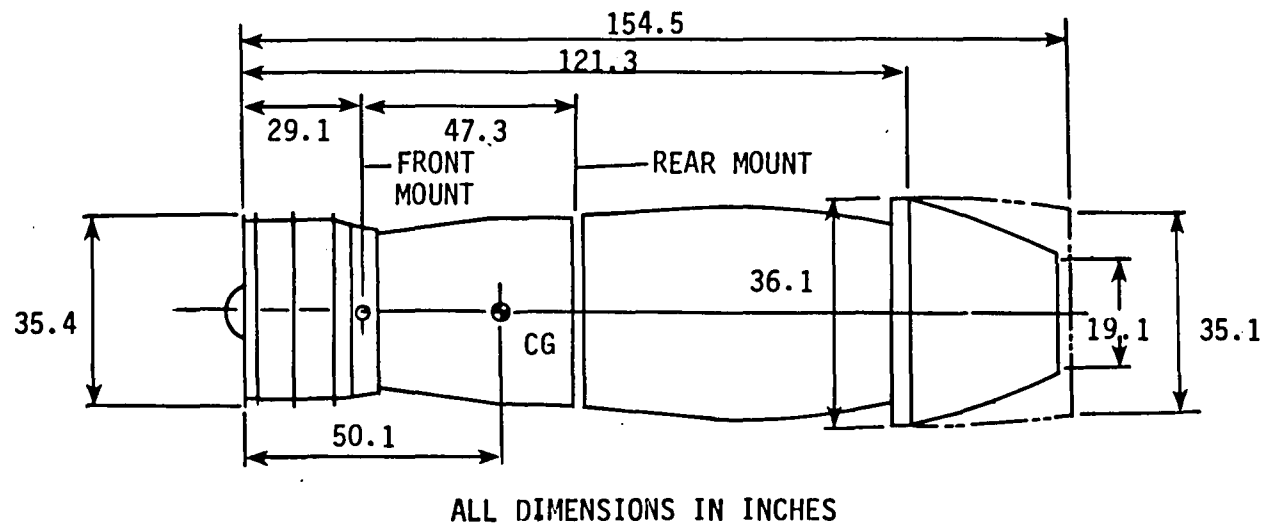
Figure III-1. - Advanced low-bypass-ratio turbofan.

PART IV. - MASS PROPERTIES

E. E. Swanson

Weight and balance analysis of the twin boom fighter was performed using a weights program based on a statistical weight estimation technique derived from correlations with advanced aircraft concepts. It was assumed that superplastic formed/diffusion bonded (SPF/DB) titanium structure would be used in all primary aircraft structure. When compared with conventional titanium structure, the following SPF/DB weight savings were incorporated (ref. IV-1):

Wing, empennage, etc.	-7%
Fuselage	-22%
Nacelle, inlet, cowling	-19%

Table IV-I presents a summary of the mass properties for the study concept at a takeoff gross weight of 47,000 lbf. Note that the maximum fuel available for the aircraft is 19,022 lbf. The aircraft center-of-gravity envelope with payload installed is presented in figure IV-1. Aircraft inertia characteristics for this study concept were not calculated. Table IV-2 summarizes the ferry fuel tank data.

REFERENCES

IV-1. Fitzsimmons, R. D.; et. al.: Technology Application Study of a Supersonic Cruise Vehicle. NASA Contractor Report 159276, March 1980.

TABLE IV-I. - GROUP WEIGHT SUMMARY

	lbf
WING	4,109
HORIZONTAL TAIL	310
VERTICAL TAIL	614
VERTICAL FIN	993
FUSELAGE	1,675
LANDING GEAR	2,031
NACELLE	3,196
STRUCTURE TOTAL	(12,928)
ENGINES	7,052
MISCELLANEOUS SYSTEMS	488
FUEL SYSTEM-TANKS AND PLUMBING	426
PROPULSION TOTAL	(7,966)
SURFACE CONTROLS	636
AUXILIARY POWER	0
INSTRUMENTS	166
HYDRAULICS	420
ELECTRICAL	715
AVIONICS	946
FURNISHINGS AND EQUIPMENT	313
AIR CONDITIONING	350
SYSTEMS AND EQUIPMENT TOTAL	(3,546)
WEIGHT EMPTY	24,440
CREW AND BAGGAGE - FLIGHT, 1	225
UNUSABLE FUEL	334
ENGINE OIL	178
OPERATING WEIGHT	25,177
PAYLOAD	4,558
ZERO FUEL WEIGHT	29,735
MISSION FUEL	17,265
TAKEOFF GROSS WEIGHT	47,000

TABLE IV-II. - FERRY FUEL TANK DATA

TANK	CAPACITY		TANK EMPTY WEIGHT
	gal	lbf	lbf
STORE-CAVITY	98.5	641	70
PALLET	450	2,925	225
PALLET	600	3,900	275

Note: All data are for a single tank. Normal ferry configurations consist of four store-cavity tanks or a pair of fuel pallets.
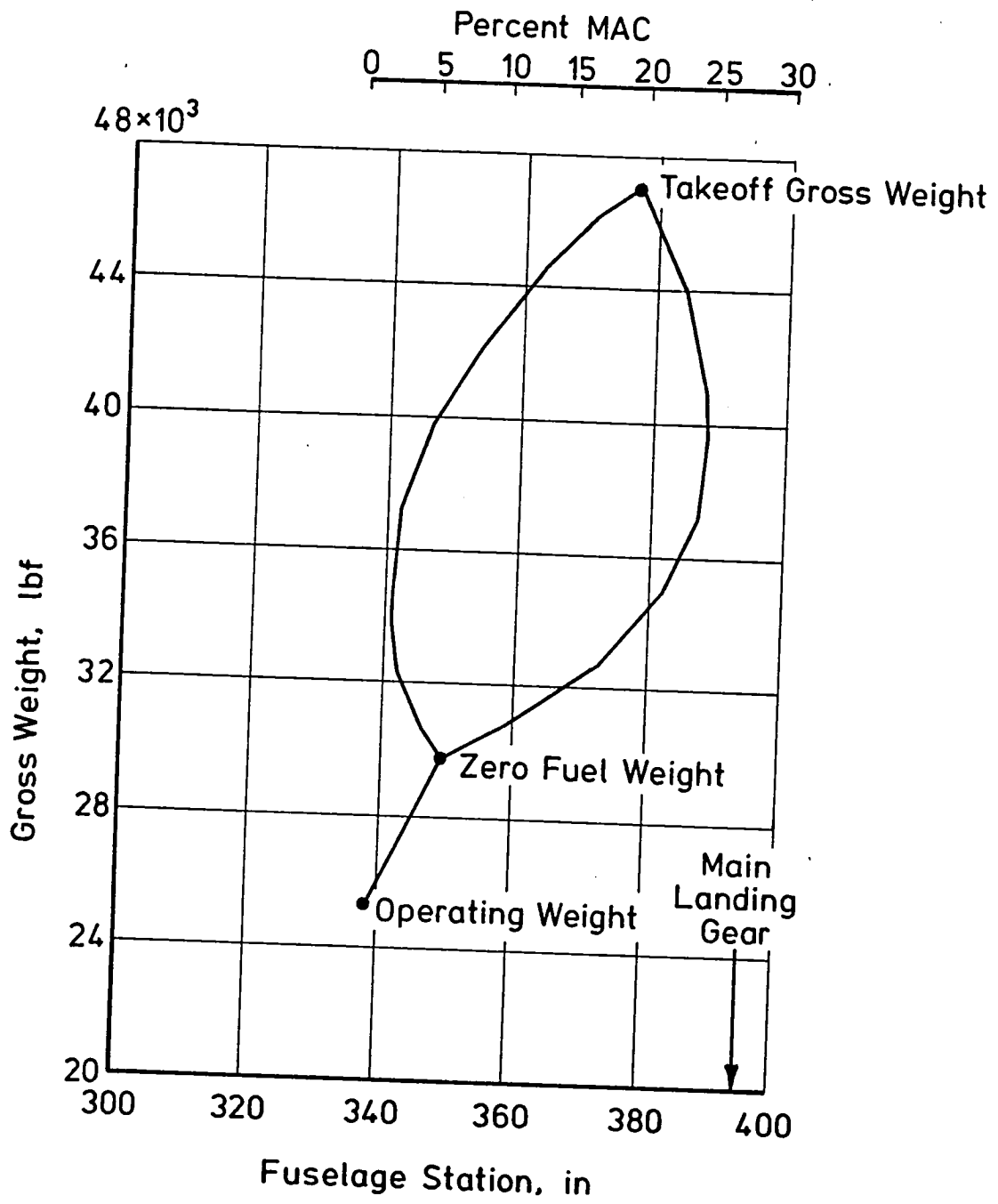
Figure IV-1. - Center-of-gravity envelope.

PART V. - AERODYNAMIC DESIGN AND ANALYSIS

K. B. Walkley and A. W. Robins

The aerodynamic design and analysis of the twin boom fighter configuration (TBF-1) has been directed toward developing a concept which exhibits high levels of supersonic cruise performance while simultaneously providing short takeoff and landing capabilities. Planform selection, propulsion system integration, wing twist and camber design, and overall configuration area distributions must be carefully integrated to achieve these performance goals. In particular, the proper matching of center-of-gravity, aerodynamic center, and nozzle hinge line locations for low-speed short field performance with thrust vectoring must be done with careful attention to maintaining low supersonic wave drag and high lift-drag ratios at cruise.

A variety of analytical methods have been used in the aerodynamic design and analysis of the TBF-1. A linearized theory technique was used to design the wing twist and camber subject to constraints on lift and pitching moment coefficients and on pressure coefficient level and gradient. Both linear and nonlinear methods were employed to determine the trimmed aerodynamic performance for Mach numbers up to 2.0.

The aerodynamic development and resulting performance for the TBF-1 are presented. Also discussed are the various methodologies employed as well as the manner in which these techniques were applied.

Symbols

a.c.   aerodynamic center

b   wing span

c   wing chord

c_D drag coefficient

20

$C_{D_{FRIC}}$ skin friction drag coefficient

$C_{D_{FORM}}$ subsonic form drag coefficient

$C_{D_{ROUGH}}$ roughness drag coefficient

$C_{D_{WAVE}}$ wave drag coefficient

$\Delta C_{D_{GEAR}}$ landing gear drag coefficient

$\Delta C_{D_{o,\ STORES}}$ zero-lift store drag coefficient

c.g.   center-of-gravity

C_L lift coefficient

$C_{L_{DES}}$ design lift coefficient

C_m pitching moment coefficient

C_{m_o} zero-lift pitching moment coefficient

$\Delta C_{m_{LINEAR}}$ incremental pitching moment coefficient from linear theory

C_p pressure coefficient

$C_{p_{LIM}}$ limiting pressure coefficient

$C_{p_{VAC}}$ vacuum pressure coefficient

c_r	wing root chord
i_{TAIL}	horizontal tail incidence angle
L/D	lift-drag ratio
$(L/D)_{MAX}$	maximum lift-drag ratio
$(L/D)_{MAX, TRIM}$	maximum trimmed lift-drag ratio
M	Mach number
r	wing leading-edge radius
S_{REF}	wing reference area
t	wing thickness
TOGW	takeoff gross weight
X, Y, Z	coordinates
x_{cg}	longitudinal location of center-of-gravity
ZFW	zero fuel weight
α_{TWIST}	wing twist angle
β	$\sqrt{M^2 - 1}$
δ_{L_1}	leading-edge flap deflection angle
δ_N	nozzle deflection angle

22

δ_{T_1}, δ_{T_2}, δ_{T_3} trailing-edge flap deflection angles

Λ_{LE} leading-edge sweep angle

Methodology

Application of the selected analytical tools focused on two areas:
(1) determination of the trimmed aerodynamic performance for Mach numbers from
0.3 to 2.0, and (2) optimization of the wing twist and camber for minimum drag at
the Mach 2.0 cruise condition. A blend of linear and nonlinear techniques were
used to determine the configuration aerodynamics for performance analysis.

Zero-Lift Drag.- Zero-lift drag was assumed to consist of supersonic wave
drag, skin friction, roughness drag, and subsonic form drag. For those cases in
which the stores were included, a base drag increment was also calculated and
included in the zero-lift drag.

Far-field wave drag was computed using the area rule method of reference V-1
as revised in reference V-2. Both stores-off and stores-on wave drag coefficients
were computed. Skin friction was estimated using the T' method of reference V-3,
and subsonic form drag values were computed using the semi-empirical relations
presented in reference V-4. An empirical relationship for the ratio of roughness
drag to skin friction drag developed in conjunction with previous supersonic
transport studies was used to estimate the roughness drag. Base drag coefficients
for the four large stores carried conformally below the wing were determined using
the procedure outlined in reference V-5. One-half of each store base was assumed
to be exposed.

Lift-Dependent Drag.- Subsonic lift-dependent drag was computed using two
methods. The vortex-lattice code described in reference V-6 was used primarily to
obtain incremental effects associated with horizontal tail deflections. Wing-alone
aerodynamics with leading- and trailing-edge flap deflections were computed using
the method described in references V-7 and V-8. The results from the wing alone
analysis were then combined with the incremental horizontal tail effects to obtain
the overall aerodynamics for Mach numbers up to 0.9.

For the supersonic Mach numbers, the program described in reference V-9 was employed. This linear theory method also included the effects of leading-edge thrust at supersonic speeds. Pitching moments as a function of lift computed with this methodology are known to be inaccurate in slope and linearity. The nonlinear methodology of reference V-10 has been shown to provide greatly improved results and was used to determine a correction to the linear theory pitching moments.

Wing Camber Surface Optimization.- The reference V-9 system of programs also includes a module for wing camber and twist optimization. A series of wing designs were generated using various constraints on lift coefficient, zero-lift pitching moment, pressure coefficient level and gradient, and design loading combinations. From these designs, a camber surface was selected for incorporation into the study concept.

Preliminary Concept

The development of the TBF-1 proceeded logically from a series of preliminary configurations. A concept that was the immediate predecessor to the TBF-1 and formed the basis from which the present configuration evolved is shown in figure V-1. The Mach 2.0 cruise performance of this configuration was less than satisfactory, but it was encouraging from the standpoint that additional performance benefits could be expected through wing camber surface optimization and other refinements to the planform and forebody. These preliminary results also indicated the potential to configure the aircraft such that at low speeds (i.e., Mach 0.3), the aerodynamic center, the center-of-gravity, and the nozzle hinge line would all have approximately the same longitudinal location. This situation could then result in significant STOL performance without the associated large trim drags typical of many STOL aircraft and without significantly compromising the supersonic cruise performance.

Parametric Aerodynamic Center Location Study
and Planform Selection

A series of planform variations relative to the preliminary configuration were investigated to establish the sensitivity of both aerodynamic center location and the Mach 2.0 lift-dependent drag. As shown in figure V-2, these planform variations included an increase in span, modifications to the trailing edge, tip panel,

24

and nozzle length, changes in the forebody geometry, and a reduction in the wing chord lengths. Combinations of some of these variations were also considered. The results of this analysis are presented in figure V-3. Planform (i) of figure V-2 was selected for the TBF-1 development. Note that the aerodynamic center has been shifted forward significantly and the Mach 2.0 C_D/C_L^2 value decreased relative to the preliminary configuration. This revised planform and the preliminary planform are compared in figure V-4. Although not included in this parametric analysis, the development of significant levels of leading-edge thrust was anticipated at the Mach 2.0 cruise due to the leading-edge shaping. The extent to which such beneficial effects were realized on the selected planform is discussed in a later section.

The Initial TBF-1 Configuration

The revised planform of figure V-4 was used as a basis for establishing the initial TBF-1 configuration shown in figure V-5. A preliminary wing twist distribution was defined and is shown in figure V-6. This twist distribution was not a result of applying the wing design code, but was instead an initial estimate. The horizontal tail geometry was essentially a fallout at this point in the development as no stability and control analysis had been conducted. A preliminary aerodynamic analysis indicated significant improvements in the Mach 2.0 cruise performance relative to the preliminary configuration. As shown in figure V-7, good performance was also estimated at Mach 1.2 and 0.8. The goal of co-locating the center-of-gravity, aerodynamic center, and nozzle hinge line at takeoff was not fully realized. The takeoff aerodynamic center (Mach 0.3) and the TOGW center-of-gravity locations are very close together, however, as shown in figure V-8.

Wing Camber Surface Design

The preliminary twist distribution defined for the initial TBF-1 provided reasonable cruise performance, but additional improvements in trimmed performance were expected from a more thorough design of the wing camber surface. The program of reference V-9 was selected to determine the wing twist and camber which would result in the maximum trimmed L/D at the Mach 2.0 cruise condition. The so-called apex loadings described in reference V-11 were used throughout the design.

The rather unusual nature of the TBF-1 configuration required a special approach to planform definition for the design process. After consideration of several alternatives, the planform shown in figure V-9 was selected. It consisted of the wing portion of the configuration together with the propulsion pod. Although it would probably not be feasible to camber the propulsion pod, a twist distribution approximating the wing design result could be incorporated and blended into the wing camber surface. This approach would only slightly compromise the optimum wing performance.

A preliminary weight analysis indicated that a reasonable design lift coefficient for the wing could be based on a weight of 35,000 pounds. For Mach 2.0 cruise at an altitude of 60,000 feet, this weight results in $C_{L_{DES}} = 0.12$. Studies concerning nonlinear supersonic aerodynamics and the effects of leading-edge thrust reported in reference V-10 point to selection of a reduced design lift coefficient for maximum L/D performance. Such a reduced $C_{L_{DES}}$ allows for a more optimum interplay of the aerodynamic benefits of both camber and leading-edge thrust at the actual flight C_L. Unfortunately, the precise value of the reduced $C_{L_{DES}}$ cannot generally be specified in advance. The camber surface resulting from the lower value will be proportionately less severe, and thus a compromise with the transonic maneuver requirement for a wing which is not too flat is also required. For the present study, a design lift coefficient of 0.08 was selected. Once the camber surface was designed, the nonlinear analysis method of reference V-10 was used to evaluate the effect of this choice.

A preliminary analysis indicated that a $C_{m_0} = 0.025$ would be required for satisfactory trim requirements, and this value was used in the initial design process. Additional values of $C_{m_0} = 0.015$ and 0.035 were considered in some detail subsequent to the initial effort in order to fully assess the impact of the C_{m_0} choice on the configuration trimmed performance for several center-of-gravity positions.

A wing thickness distribution consisting of a series of modified NACA 65A sections was defined. The thickness variation with semispan fraction shown in figure V-10 was selected to provide adequate fuel volume and low wave drag. The sections were flattened somewhat on the lower surface in the vicinity of the wing-mounted stores to facilitate the conformal carriage arrangement. Sharp

leading edges were incorporated for the inboard portion of the wing where the leading edge is supersonic.

The wing design code of reference V-9 also allows specification of wing upper surface pressure level and gradient constraints. The design code cycles until these constraints are satisfied, or, under certain conditions, until a reduced constraint is satisfied. A pressure level constraint of $C_{P_{LIM}} \geq .75 \, C_{P_{VAC}}$ and a gradient constraint of $dC_P/dX \leq .0050$ per foot were selected.

Initial attempts to design the wing to a pressure coefficient gradient constraint of $dC_P/dX \leq .0050$ per foot led to unacceptable camber shapes for the wing resulting in excessive drag levels. It was therefore necessary to relax this constraint to a value of .0180 per foot to achieve an acceptable design solution. The impact of this greater gradient on possible flow separation was not evaluated.

The selected camber surface is illustrated in figure V-11. These camber lines were sheared vertically to provide straight trailing-edge flap hinge lines lying in the horizontal wing reference plane. Figure V-12 presents a series of cross sections through the sheared wing with the thickness envelope added.

The choice of $C_{L_{DES}}$ was evaluated for the selected camber surface using the nonlinear method of reference V-10. These results are presented in figure V-13. A series of wing camber surfaces corresponding to design lift coefficients of 0., 0.04, 0.12, and 0.16 were defined by scaling the previously developed camber values by the ratio of the desired $C_{L_{DES}}$ to 0.08. Thus, the $C_{L_{DES}} = 0.16$ camber values are twice those of the original design. Each of these wings was then analyzed and an $(L/D)_{MAX}$ value computed using the zero-lift drag values obtained for the initial TBF-1 geometry. The results presented in figure V-13 indicated that the best wing would be obtained for $C_{L_{DES}} = 0.04$, and that the $(L/D)_{MAX}$ performance decreases rapidly as the wing $C_{L_{DES}}$ increases. The initial choice of $C_{L_{DES}} = 0.08$ appears to be a reasonable selection as only a small penalty is incurred relative to the optimum, and there should be sufficient camber and twist in the wing to provide sufficient self-trimming moment (C_{m_0}) at cruise as well as reasonable transonic maneuver performance.

Trim Considerations

As previously noted, a pitching moment constraint of $C_{m_0} = .025$ was used in the wing design study. In order to more fully assess the impact of this C_{m_0} choice on the configuration trimmed aerodynamic performance, additional wing design solutions were obtained with C_{m_0} constraints of .015 and .035. A trim analysis was then conducted for assumed center-of-gravity locations of x_{cg} = 360., 370., 380., and 387. inches. Rather than directly using the linear theory pitching moment results obtained from reference V-9, the nonlinear method of reference V-10 was employed as illustrated in figure V-14. The linear theory solution was used to determine the incremental effect of adding the horizontal tail at a given incidence. These increments were then applied to the nonlinear solution for the wing alone to obtain a more accurate representation of the tail-on pitching moment. A typical trim diagram obtained using this combination of linear and nonlinear methodology is shown in figure V-15. Trimmed drag polars were then constructed from the linear theory solutions (including attainable leading-edge thrust), and the $(L/D)_{MAX}$ values were determined. Figure V-16 summarizes these results. Trimmed performance for the wing with the preliminary twist distribution is below that of each of the other wing designs. The $C_{m_0} = .025$ results are best for the aft center-of-gravity locations, and again represent the wing design of choice.

Attainable Leading-Edge Thrust

Throughout the analysis of the TBF-1, the computed drag-due-to-lift results have included the effects of attainable leading-edge thrust, and the wing planform selection was influenced in part by a desire to provide for the achievement of leading-edge thrust. (For a complete discussion of the thrust analysis procedure, see reference V-12. Additional discussions relative to supersonic planforms which develop significant levels of leading-edge thrust may be found in reference V-13.) The selection of a reduced design lift coefficient for the wing design also reflects the influence of leading-edge thrust. As shown in reference V-10, the "best" wing will include the effects of both camber (i.e., distributed thrust) and leading-edge thrust. To illustrate the effect of leading-edge thrust on the performance of the present configuration, an analysis of the selected wing design was conducted.

Figure V-17 presents the spanwise distribution of leading-edge sweep angle and radius. The radius values for NACA 65A003 and 65A004 airfoil sections are noted. Also shown is the distribution of the parameter $1/\beta\cot\Lambda_{LE}$ which is the ratio of the tangent of the leading-edge sweep angle to the tangent of the sweep of the Mach line. For values of $1/\beta\cot\Lambda_{LE}$ equal to or less than unity, the leading-edge is supersonic and no thrust can be developed. Subsonic leading-edges correspond to values greater than unity. If sufficient leading-edge radius is provided when $1/\beta\cot\Lambda_{LE}>1$, then significant leading-edge thrust levels can be achieved. As figure V-17 shows, sufficient leading-edge radii were provided in a manner consistent with the $1/\beta\cot\Lambda_{LE}$ distribution for the Mach number indicated.

The impact of the actual levels of leading-edge thrust on the aerodynamic performance is shown in figure V-18 for Mach numbers 2.0 and 1.2. Shown are untrimmed drag polars with 0 percent, 100 percent, and attainable leading-edge thrust levels. Also presented for the Mach 2.0 case is the flat wing solution with no leading-edge thrust. The tabulated $(L/D)_{MAX}$ values illustrate the performance benefits associated with the various levels of thrust. It is noteworthy that at Mach 2.0, nearly 100 percent thrust levels were obtained, and the $(L/D)_{MAX}$ value is only 0.07 below the full thrust result. At Mach 1.2, a significant increase in $(L/D)_{MAX}$ was achieved through inclusion of the thrust effect, but a smaller portion of the full thrust was obtained than was the case at Mach 2.0.

The TBF-1 Baseline Configuration

The results obtained for the initial TBF-1 configuration established both the analysis methodologies and the configuration details. This initial configuration was then refined and a more detailed aerodynamic analysis performed for Mach numbers from 0.3 to 2.0. This revised configuration is designated the TBF-1 baseline configuration.

Revisions to the initial TBF-1 included: (1) modifications to the horizontal tail planform and area to obtain a volume coefficient more consistent with current fighters; (2) incorporation of the $C_{m_0} = .025$ wing camber and twist distribution; and (3) increased boom volume to provide additional fuel capacity. The additional wing span associated with the rail launcher located on the wing tips was also included in the analysis. Figure V-19 illustrates the wing span and horizontal tail changes.

Modifications to the boom geometry were accomplished through careful area ruling of the booms in conjunction with the remainder of the configuration components. Approximately 1,500 pounds of additional fuel was added to the TBF-1 without incurring a wave drag penalty at cruise. Only very small changes in wave drag occurred at the other supersonic Mach numbers. A numerical model representation of the baseline configuration is shown in figure V-20.

High Speed Aerodynamics

Trimmed high-speed drag polars for the TBF-1 baseline were established for the climb profile shown in figure V-21. At the subsonic Mach numbers the center-of-gravity was fixed at $x_{cg} = 375.$ inches, whereas it was $x_{cg} = 380.$ inches for the supersonic condition. As shown in the Mass Properties section, subsequent design iterations for this baseline configuration resulted in a balance diagram for which these center-of-gravity locations are not achievable at the lower weight conditions. The aerodynamic performance levels to be presented include trim drag associated with these assumed center-of-gravity locations, but no attempt was made to optimize center-of-gravity location in conjunction with the trimmed aerodynamic performance.

The variation of skin friction, form, and roughness drag for the baseline configuration is presented in figure V-22, and the zero-lift wave drag values are shown in figure V-23. Except as noted, these curves are all for the stores-off and missile launcher-on condition. The zero-lift drag increment due to the stores - including base drag - is shown as a function of Mach number in figure V-24. Typical trimmed polars are presented in figure V-25 with operating points noted. Table V-1 presents a complete set of polars for the baseline configuration. Both stores-on and -off trimmed $(L/D)_{MAX}$ results are summarized in figure V-26. At the Mach 2.0 cruise condition, the stores-on trimmed $(L/D)_{MAX}$ value is 6.25.

High-Lift Configuration

A Mach 0.3 polar was established for use in the takeoff and landing performance analysis. A nominal high-lift configuration was defined with the leading-edge flap deflected $\delta_{L_1} = 20°$, the inboard trailing-edge flaps at $\delta_{T_1} = \delta_{T_2} = 20°$, and the flaperon at $\delta_{T_3} = 10°$. The nozzle deflection angle was assumed to be $\delta_N = 30°$ and a flap was included to simulate the power-off effect

of this deflected surface. Trimmed polars were computed using the techniques previously discussed. Figure V-27 presents the flap geometry, and figure V-28 shows the resulting polar out of ground effect with the gear up. Table V-II presents the corresponding numerical values for the polar. An estimate of the gear drag is indicated. Flap deflections were not optimized for this analysis and additional improvements in the low-speed performance may be possible.

Aerodynamic Center

Figure V-29 presents the rigid airplane aerodynamic center and center-of-gravity relationships for the baseline TBF-1. Note that the configuration is stable throughout the flight envelope. Although somewhat more aft locations of the TOGW and ZFW centers-of-gravity were desired, a reasonable relationship between the centers-of-gravity, nozzle hinge line, and aerodynamic centers has been achieved for the baseline configuration. Additional configuration design work should be able to more nearly achieve the desired co-location of aerodynamic center, center of gravity, and nozzle hinge lines.

Power-On Effects

Power effects on the aerodynamic performance have not been included in the present analyses of the TBF-1. Three such effects - thrust induced lift due to supercirulation, persistence of the downwash sheet associated with the deflected nozzle, and exhaust plume bouyancy effects on the twin booms - are of particular interest. All of these effects offer the possibility of significantly improving the aerodynamic performance.

Fuel Pallet Drag

The two fuel pallets developed to provide additional fuel capacity for various ferry missions provide either 450 or 600 gallons of additional fuel each and are carried conformally beneath the wing as shown in figure II-8 of the Configuration Description section. The area distribution of the pallets was tailored to provide minimal wave drag penalties at Mach 1.4 for a supersonic ferry mission. Figure V-30 presents the zero-lift drag increment associated with these pallets. For subsonic Mach numbers the drag increment is simply that due to a slight increase in wetted area. At supersonic speeds, the wave drag increments are also included.

Maneuver Polars

A maneuver polar was determined for Mach 0.9 at an altitude of 26,500 feet using the theoretical method of references V-7 and V-8. For a range of lift coefficients, the flap deflection combination which resulted in the lowest drag due to lift was determined. An envelope polar was then constructed through these optimum points. The resulting maneuver polar and flap deflection schedule is shown in figure V-31.

REFERENCES

V-1.   Harris, Roy V., Jr.: An Analysis and Correlation of Aircraft Wave Drag. NASA TM X-947, 1964.

V-2.   Craidon, Charlotte B.: User's Guide for a Computer Program for Calculating the Zero-Lift Wave Drag of Complex Aircraft Configurations. NASA TM-85670, 1983.

V-3.   Sommer, Simon C.; and Short, Barbara J.: Free Flight Measurements of Turbulent Boundary Layer Skin Friction in the Presence of Severe Aerodynamic Heating at Mach Numbers from 2.8 to 7.0. NACA TN 3391, 1955.

V-4.   Hoerner, S. F.: Fluid Dynamic Drag. Hoerner Fluid Dynamics, 1965.

V-5.   Honeywell, E. E.: Compilation of Power-Off Base Drag Data and Empirical Methods for Predicting Power-Off Base Drag. Convair Report No. TM-334-337, 1959.

V-6.   Miranda, Luis R.; Elliot, Robert D.; and Baker, William M.: A Generalized Vortex Lattice Method for Subsonic and Supersonic Flow Applications. NASA CR-2865, 1977.

V-7.   Carlson, Harry W.; and Walkley, Kenneth B.: A Computer Program for Wing Subsonic Aerodynamic Performance Estimates Including Attainable Thrust and Vortex Lift Effects. NASA CR-3515, 1982.

V-8.   Carlson, Harry W.; and Walkley, Kenneth B.: An Aerodynamic Analysis
        Computer Program and Design Notes for Low Speed Wing Flap Systems. NASA CR-
        3675, 1983.

V-9.   Middleton, W. D.; Lundry, J. L.; and Coleman, R. G.: A System for
        Aerodynamic Design and Analysis of Supersonic Aircraft. 4 Volumes, NASA CR-
        3351, 3352, 3353, and 3354, 1980.

V-10.   Carlson, Harry W.; and Mack, Robert J.: Estimation of Wing Nonlinear
        Aerodynamic Characteristics at Supersonic Speeds. NASA TP-1718, 1980.

V-11.   Miller, David S.; and Schemensky, Roy T.: Design Study Results of a
        Supersonic Cruise Fighter Wing. AIAA Paper 79-0062, 1979.

V-12.   Carlson, Harry W.; Mack, Robert J.; and Barger, Raymond L.: Estimation of
        Attainable Leading-Edge Thrust for Wings at Subsonic and Supersonic Speeds.
        NASA TP-1500, 1979.

V-13.   Robins, A. Warner; Carlson, Harry W.; and Mack, Robert J.: Supersonic Wings
        with Significant Leading-Edge Thrust at Cruise. NASA TP-1632, 1980.

TABLE V-I. - HIGH SPEED TRIMMED DRAG POLARS.
S_{REF} = 677 FT^2, x_{cg} = 380.0 IN., STORES OFF.

MACH NO. ALTITUDE, FT C_L	2.0 60,000 C_D	2.0 48,240 C_D	1.8 44,800 C_D	1.6 41.300 C_D	1.4 37,700 C_D	1.2 34,300 C_D
0.	.0229	.0221	.0229	.0238	.0228	.0211
.02	.0223	.0216	.0225	.0234	.0226	.0210
.04	.0220	.0213	.0224	.0234	.0225	.0212
.06	.0221	.0214	.0226	.0235	.0228	.0216
.08	.0226	.0218	.0230	.0238	.0231	.0221
.10	.0234	.0226	.0237	.0244	.0236	.0227
.12	.0245	.0238	.0246	.0252	.0244	.0235
.14	.0259	.0252	.0258	.0261	.0253	.0245
.16	.0277	.0269	.0273	.0274	.0264	.0255
.18	.0296	.0289	.0290	.0289	.0278	.0268
.20	.0318	.0312	.0311	.0307	.0294	.0282
.22	.0345	.0338	.0333	.0328	.0311	.0298
.24	.0373	.0367	.0359	.0351	.0332	.0298
.26	.0405	.0398	.0387	.0376	.0355	.0317
.28	.0441	.0433	.0419	.0403	.0380	.0337
.30	.0479	.0470	.0454	.0436	.0407	.0360
.32	.0521	.0510	.0489	.0466	.0437	.0385
.36	.0607	.0594	.0568	.0537	.0502	.0413
.40	.0697	.0682	.0651	.0619	.0576	.0475
						.0559

TABLE V-I. - CONCLUDED.

$$x_{cg} = 375.0 \text{ IN.}$$

MACH NO.	0.9	0.8	0.6
ALTITUDE, FT	26,500	20,500	7,000
C_L			
0.	.0108	.0107	.0110
.02	.0109	.0107	.0112
.04	.0112	.0110	.0114
.06	.0115	.0114	.0117
.08	.0122	.0118	.0123
.10	.0127	.0125	.0128
.12	.0135	.0134	.0136
.14	.0144	.0144	.0146
.16	.0155	.0154	.0158
.18	.0167	.0168	.0173
.20	.0183	.0184	.0189
.24	.0219	.0221	.0227
.28	.0266	.0267	.0273
.32	.0322	.0322	.0328
.36	.0386	.0386	.0397
.40	.0462	.0459	.0477
.45	.0573	.0571	.0588
.50	.0703	.0698	.0717
.55	.0844	.0847	.0863
.60	.1003	.1007	.1023
.65	.1175	.1182	.1200

TABLE V-II. - LOW-SPEED TRIMMED DRAG POLAR.
GEAR UP, OUT OF GROUND EFFECT,
$\delta_{L_1} = 20°$, $\delta_{T_1} = \delta_{T_2} = 20°$, $\delta_{T_3} = 10°$,

$\delta_N = 30°$ POWER OFF

$S_{REF} = 677$ FT^2, $x_{cg} = 373$ IN.

MACH NO.	0.3
ALTITUDE, FT	0.
C_L	C_D
0.	.0582
.05	.0532
.10	.0497
.15	.0477
.20	.0479
.25	.0496
.30	.0529
.35	.0574
.40	.0625
.45	.0686
.50	.0759
.55	.0843
.60	.0943
.70	.1210
.80	.1550

$\Delta C_{D_{GEAR}} = .0150$
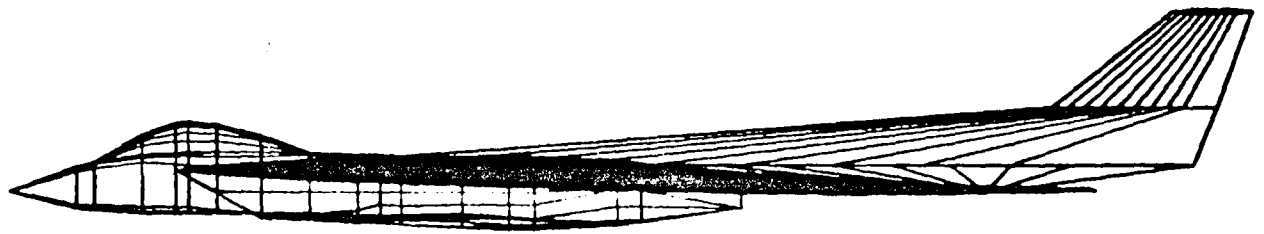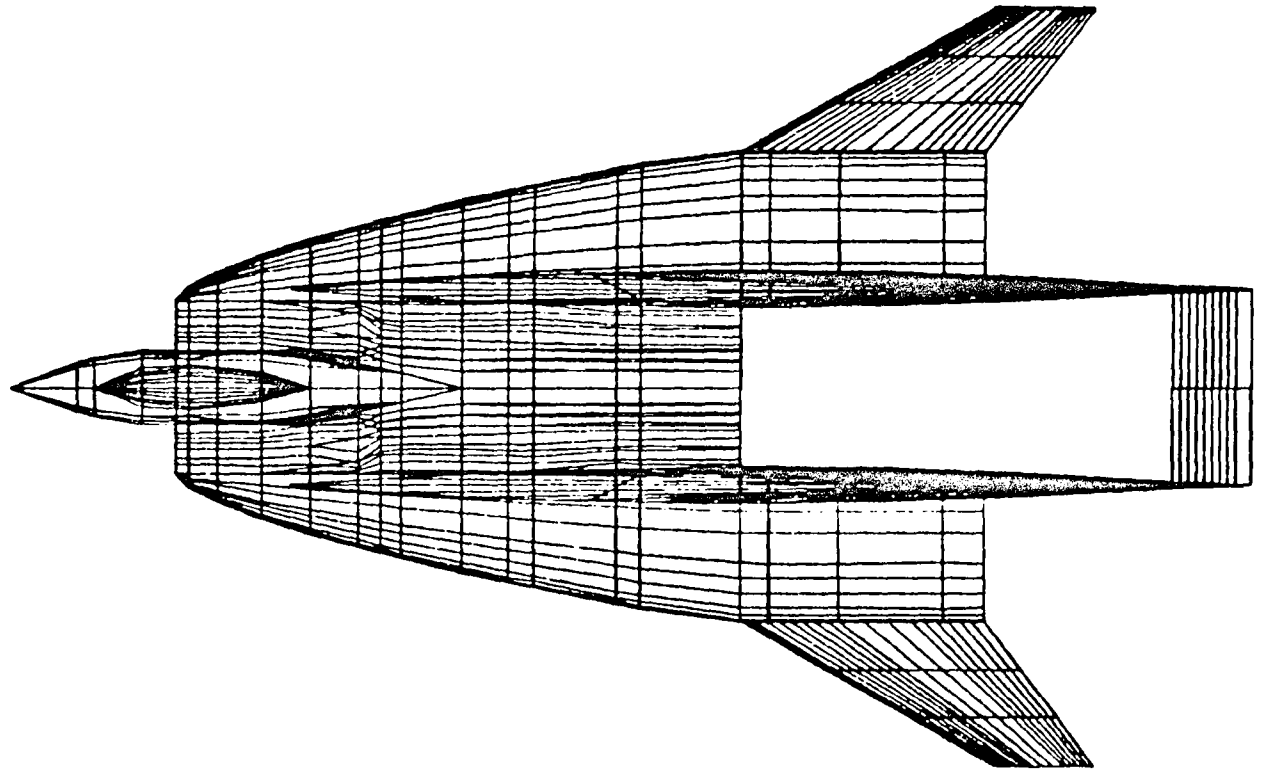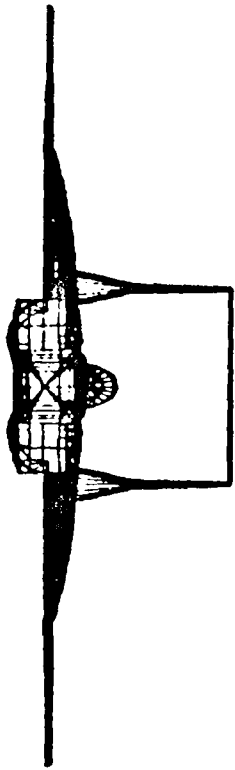
Figure V-1. - The preliminary configuration.

Note: Dashed lines show the preliminary planform.

(a) Increased span

(b) Modified trailing edge

(c) Modified tip panel

(d) Modified nozzle

(e) Modified chord distribution

(f) Combination of (a) and (b)

(g) Modified leading edge with (a) and (b) and forebody extension

(h) Combination of (g) and (e) with $\Lambda_{tip} = 60°$

(i) Configuration (h) with $\Lambda_{tip} = 62°$
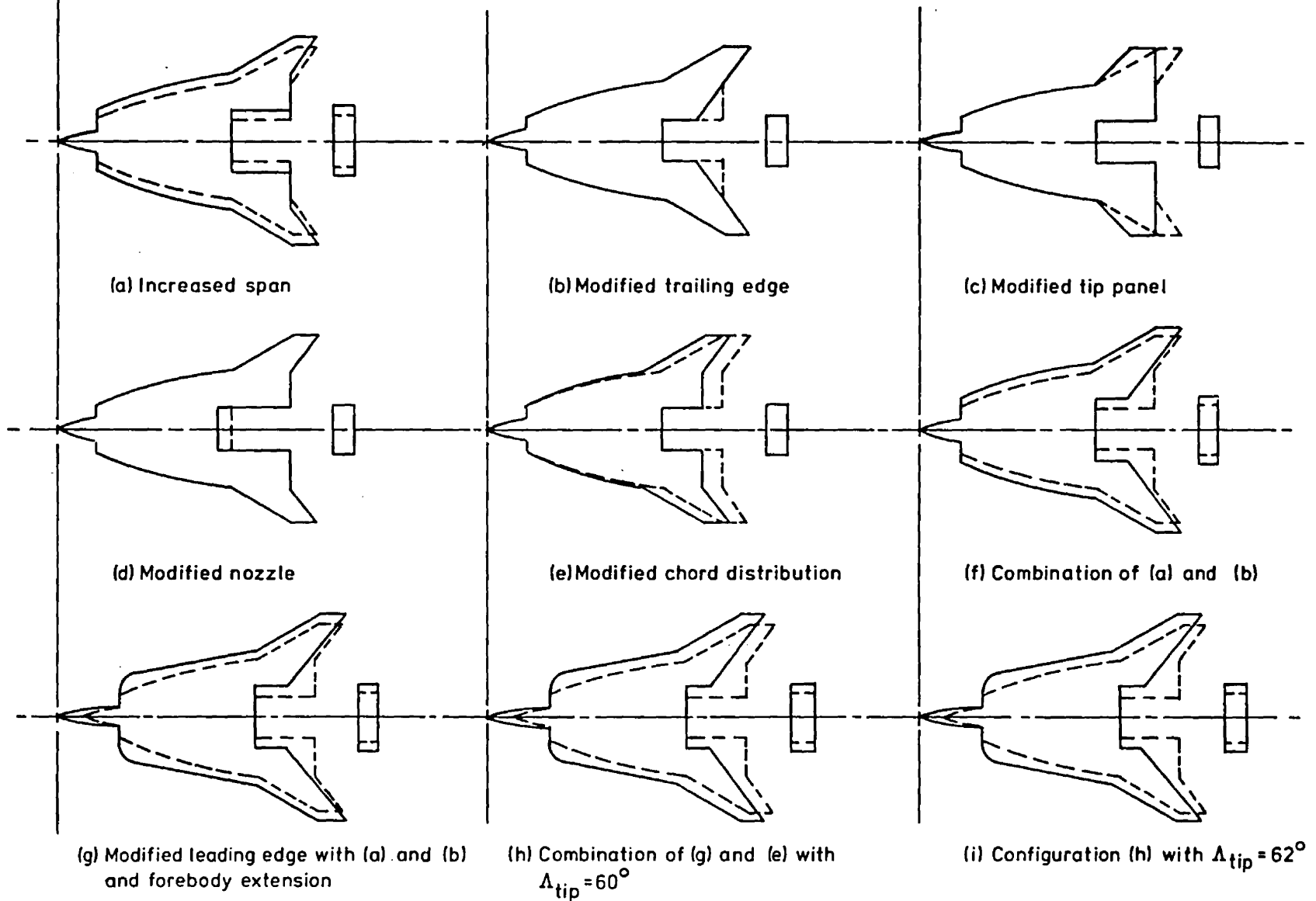
Figure V-2. - Planforms for parametric aerodynamic center location study.
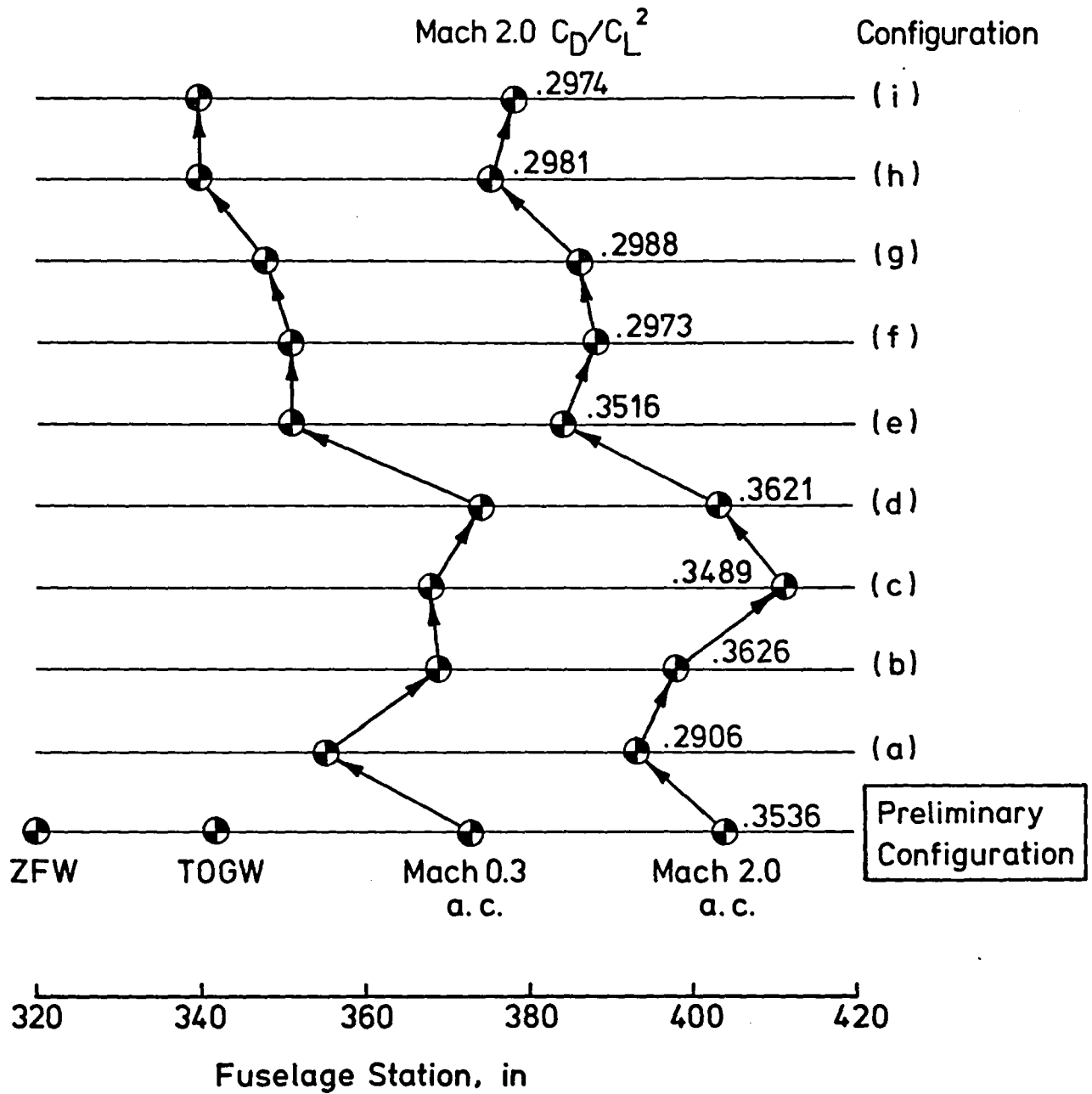
Figure V-3. - Aerodynamic center and lift-dependent drag variations.
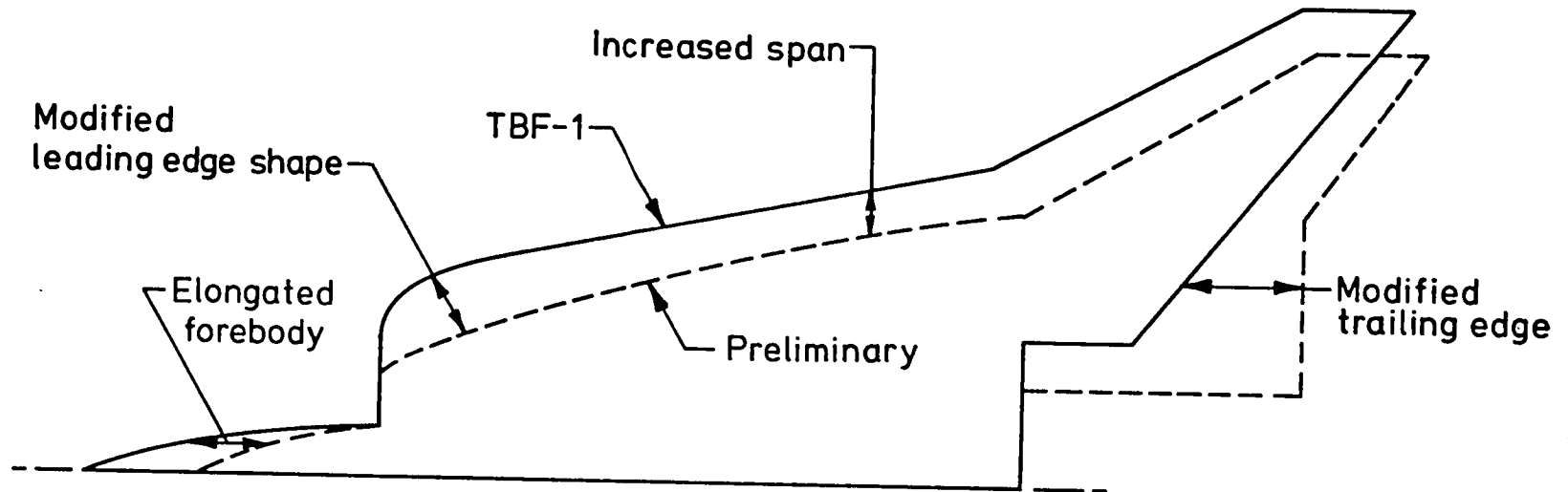
Figure V-4. - Preliminary configuration and TBF-1 planform comparison.
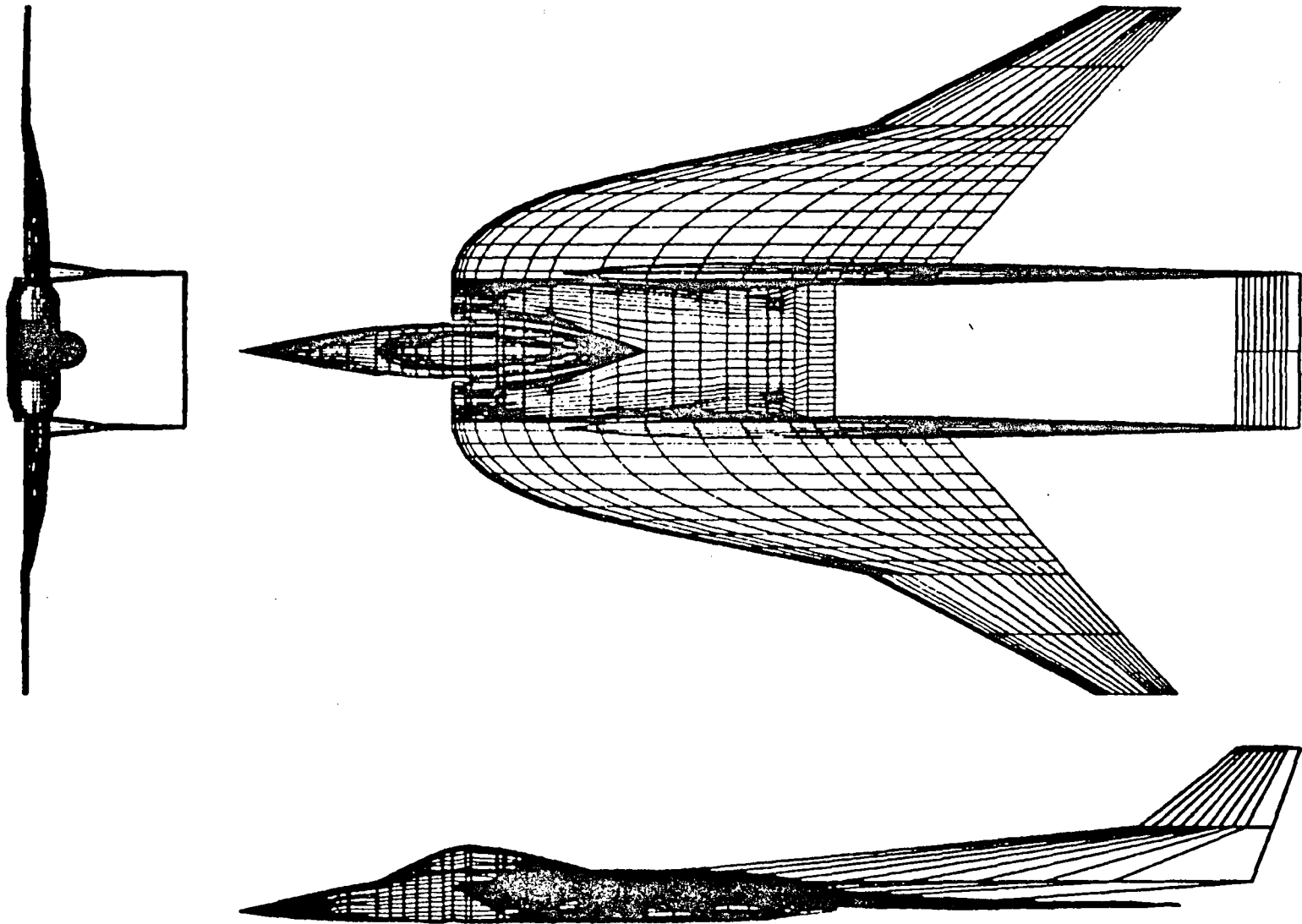
Figure V-5. - Initial TBF-1 configuration.
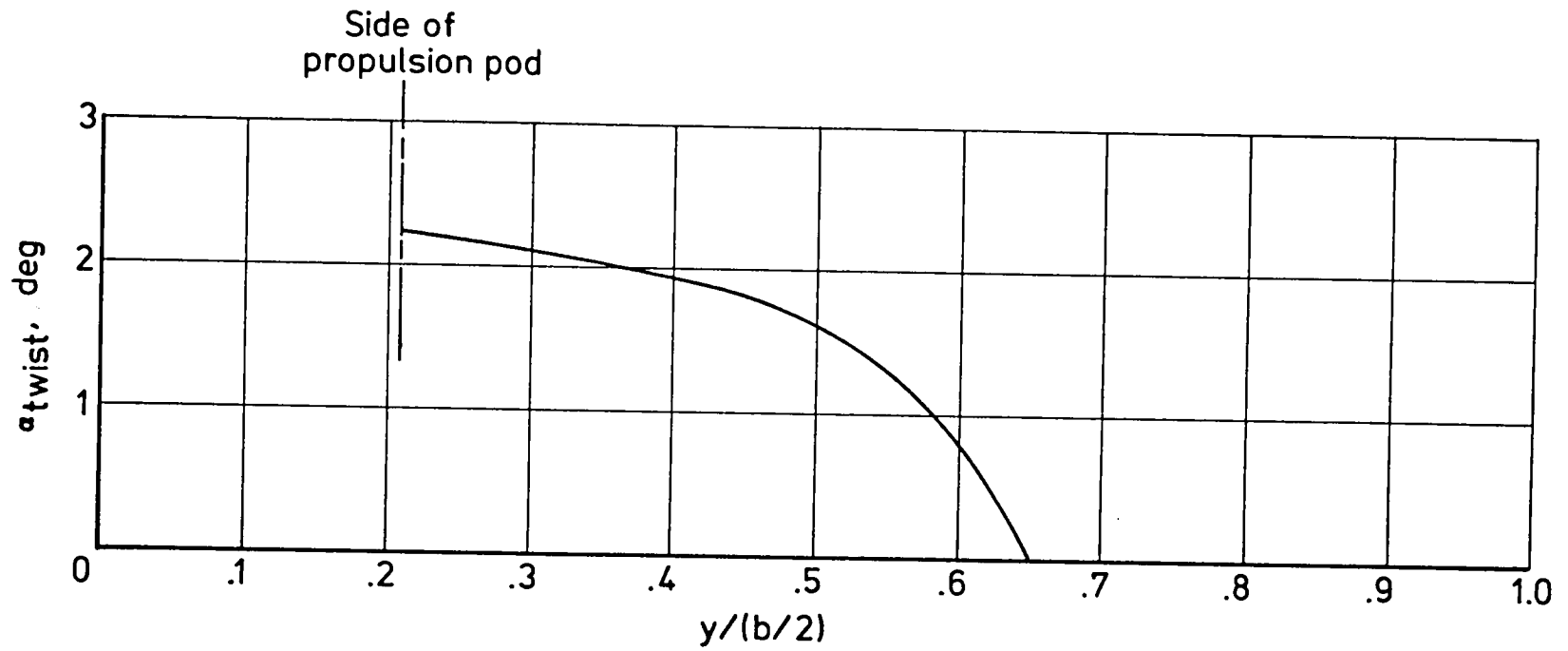
Figure V-6. – Preliminary wing twist distribution.
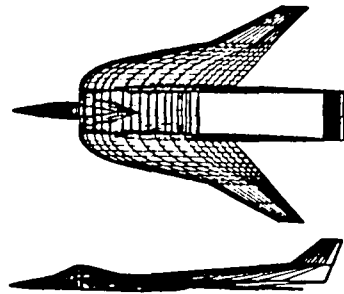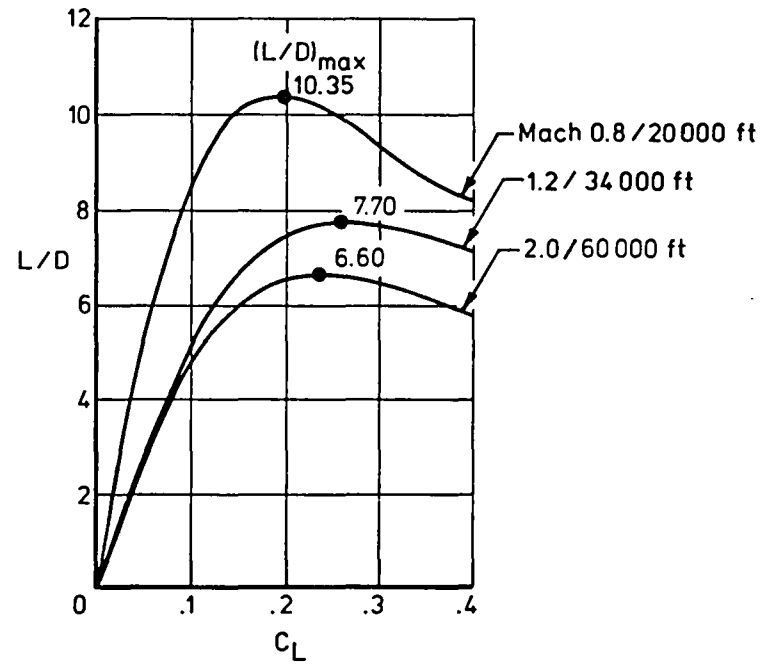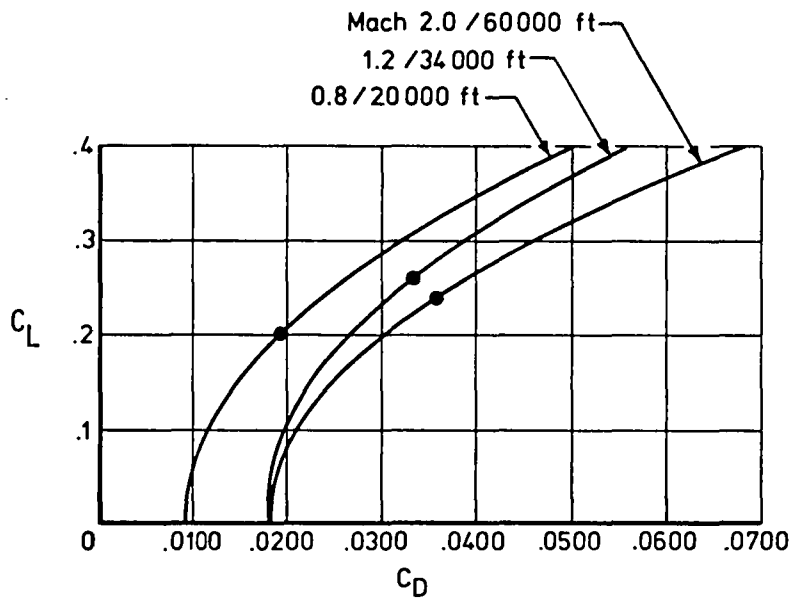
Figure V-7. — Aerodynamic performance for the initial TBF-1 configuration.

M 0.3
M 0.8
M 1.2
M 2.0

a.c's

c.g's
TOGW
ZFW
OWE

2-D Nozzle Hinge Line
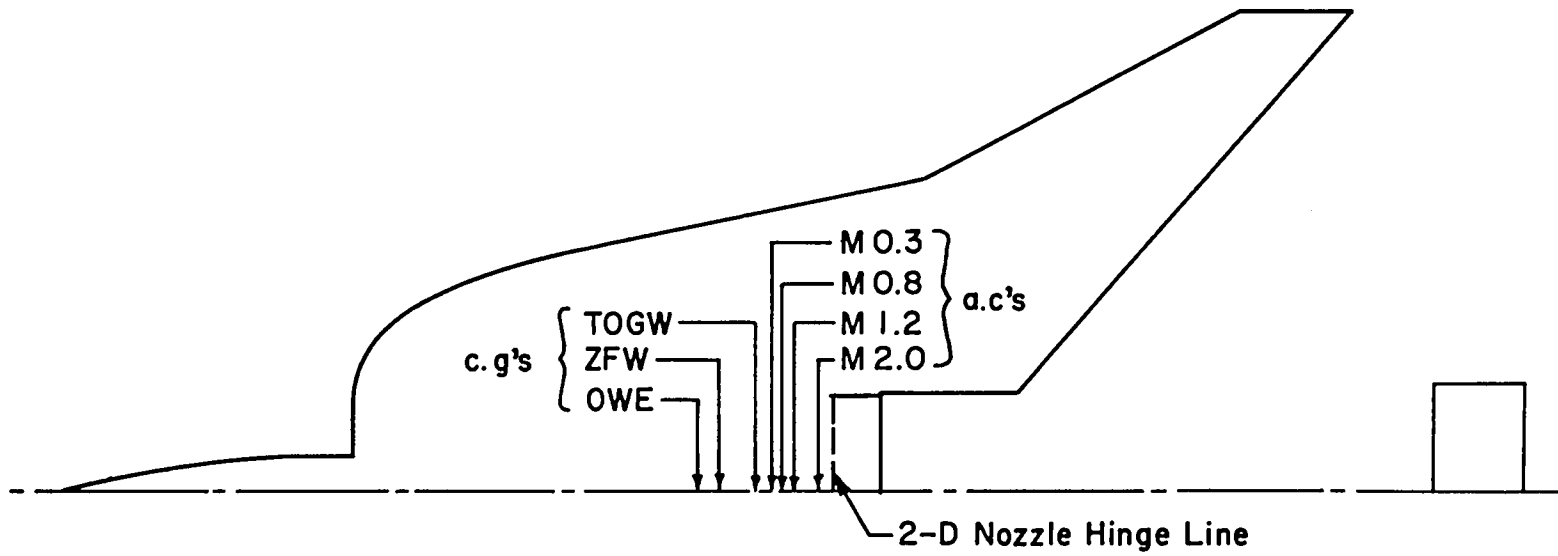
Figure V-8. - Aerodynamic centers and center-of-gravity for the
initial TBF configuration.
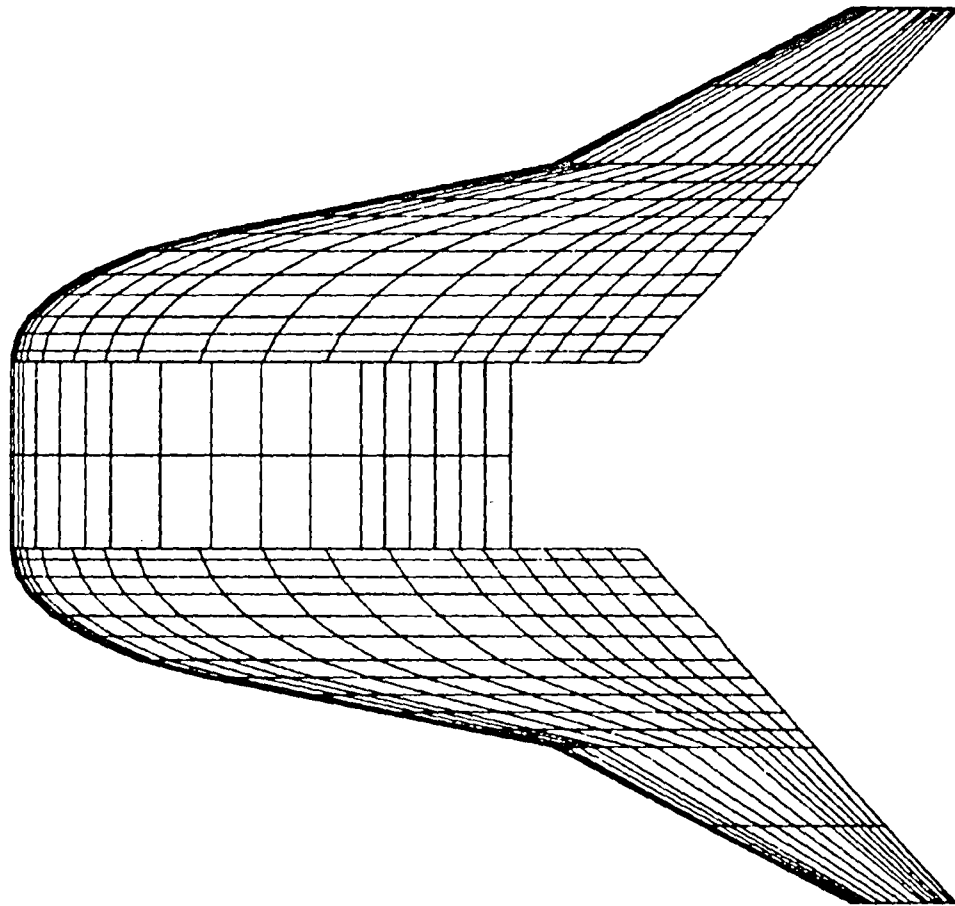
Figure V-9. - Planform for wing design.
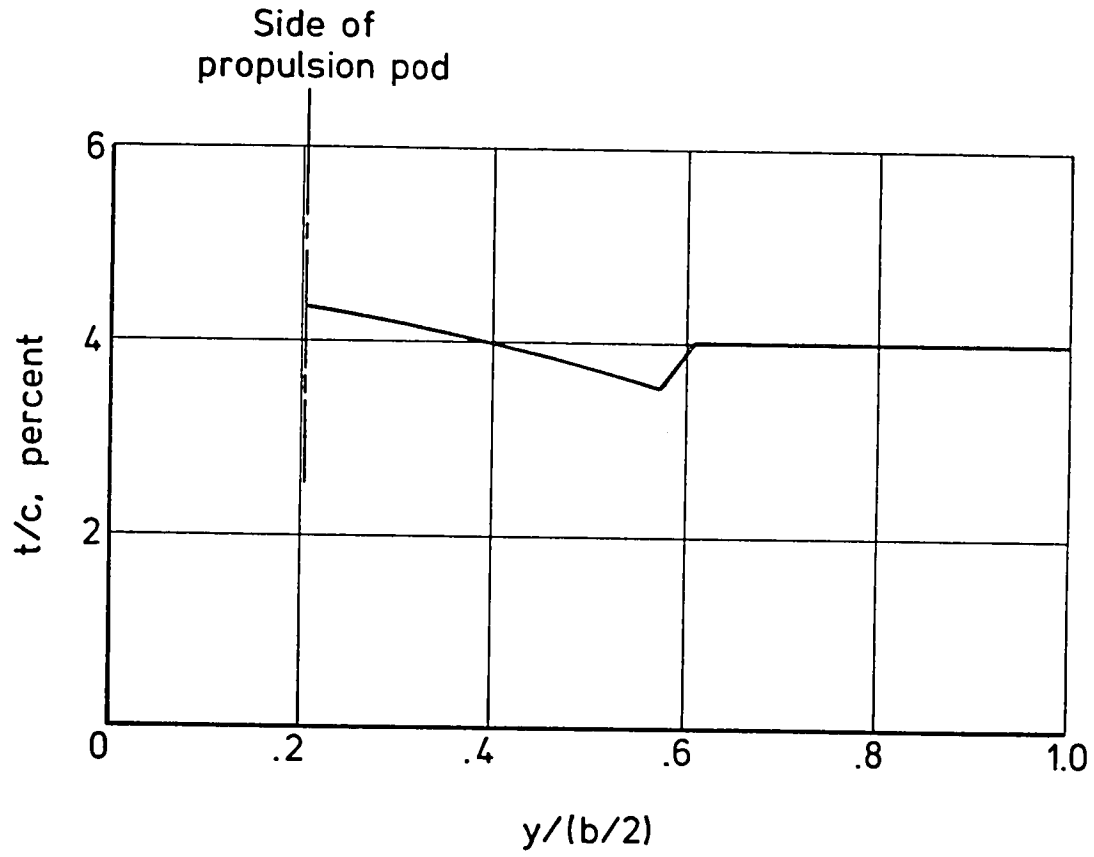
Figure V-10. - Wing thickness distribution.
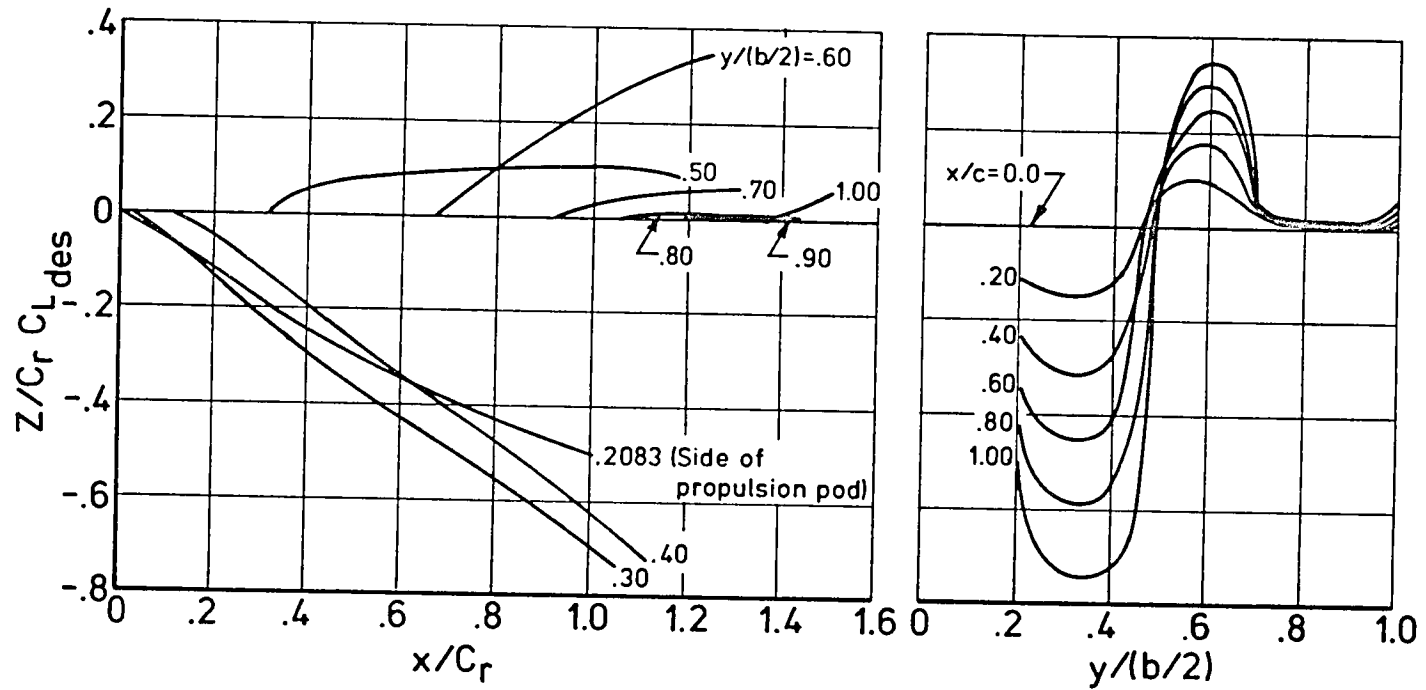
Figure V-11. - Camber surface of wing with respect to the leading edge.
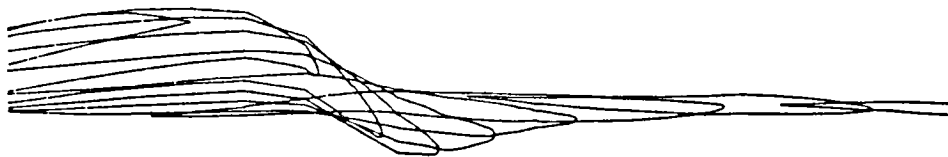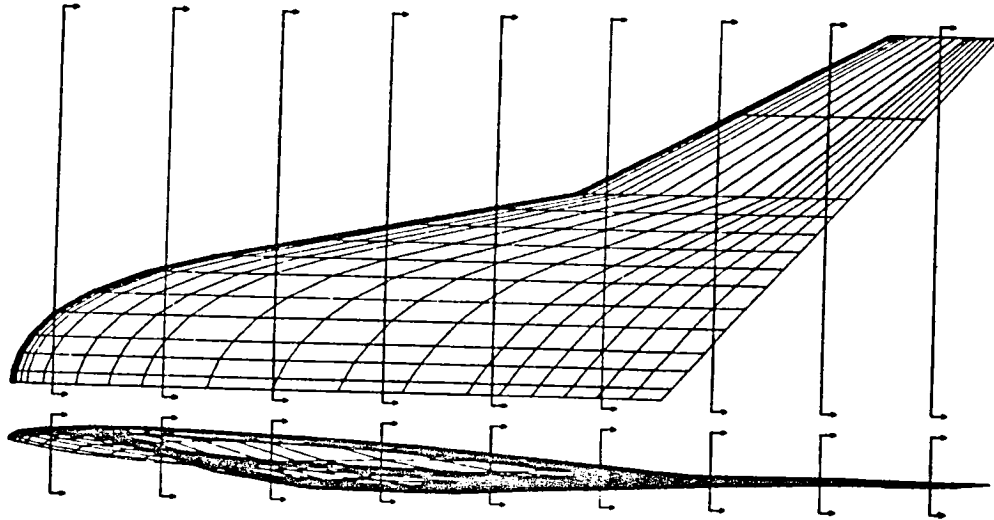
Figure V-12. - Selected camber surface sheared and thickness added.
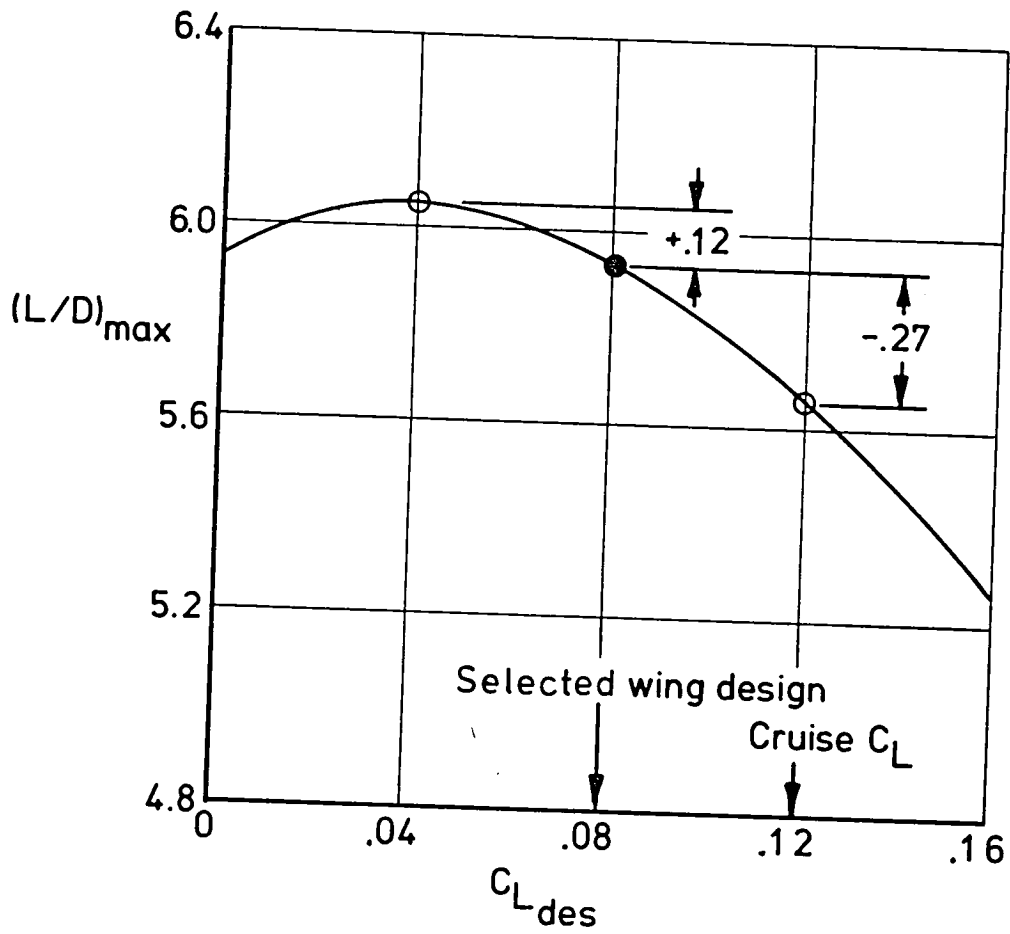
Figure V-13. - Effect of $C_{L_{DES}}$ on $(L/D)_{MAX}$ performance at Mach 2.0.
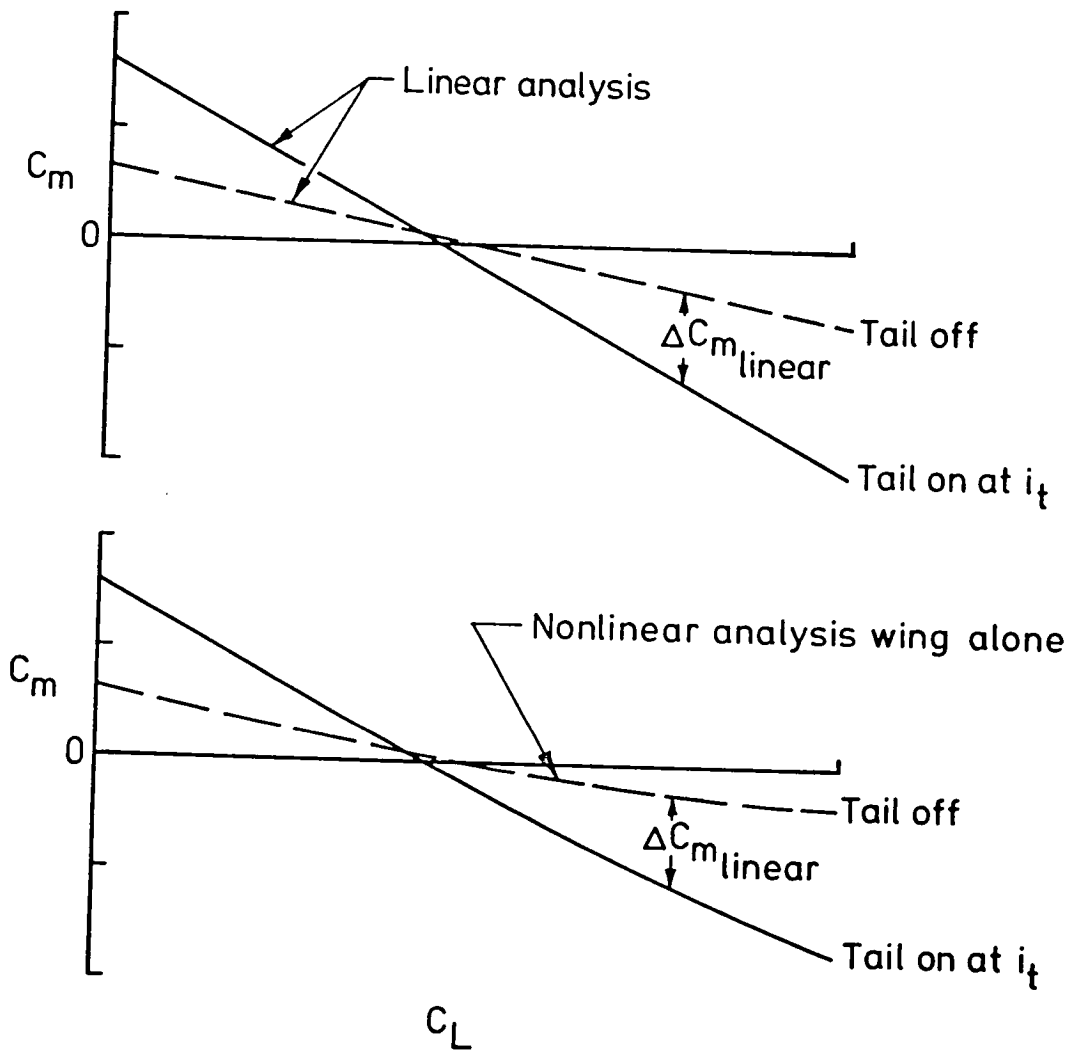
Figure V-14. - Supersonic trim analysis procedure using nonlinear analysis for the wing alone solution.
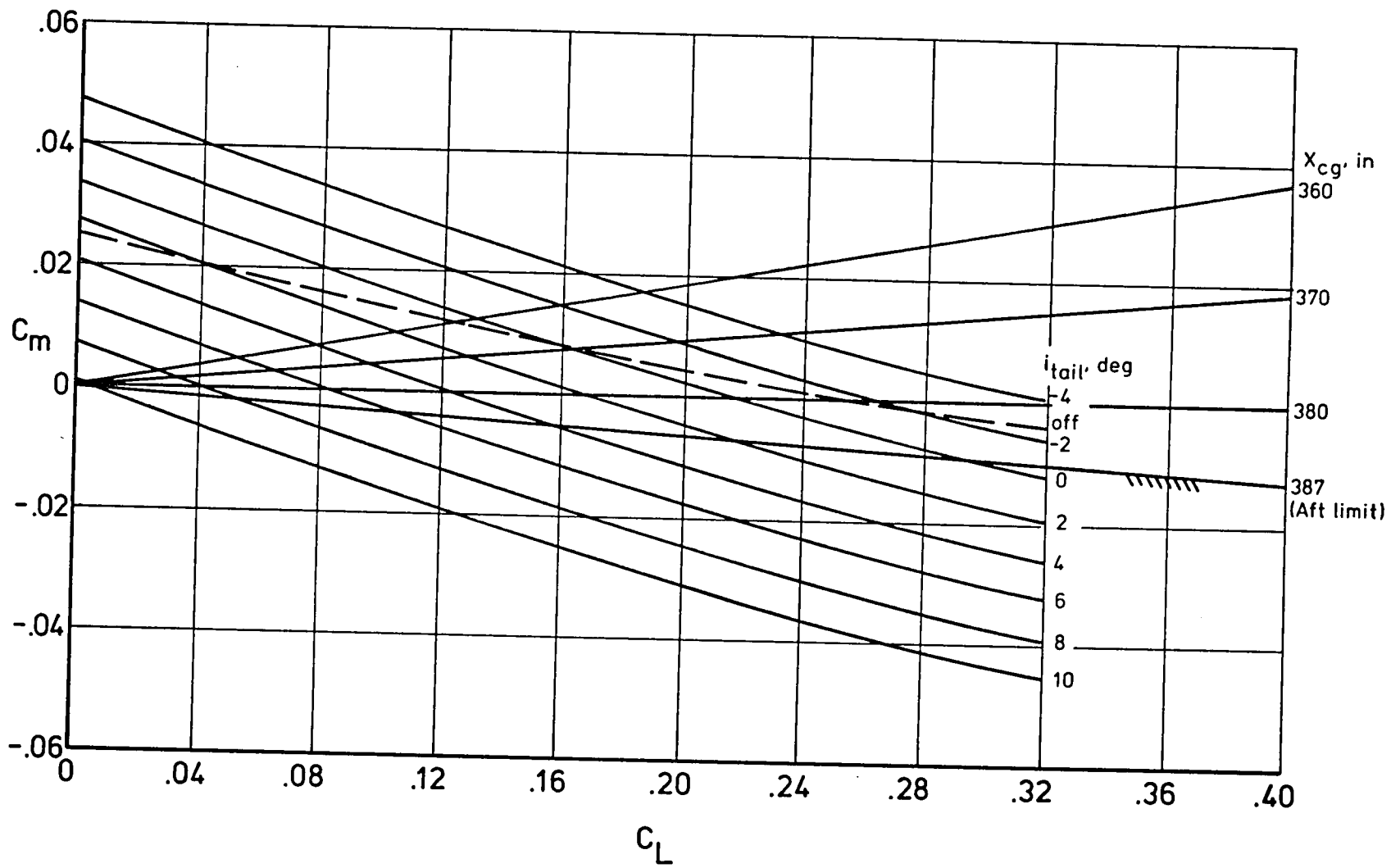
Figure V-15. - Typical Mach 2.0 trim diagram obtained from linear
and nonlinear methodologies.

Mach 2.0, 60 000 ft
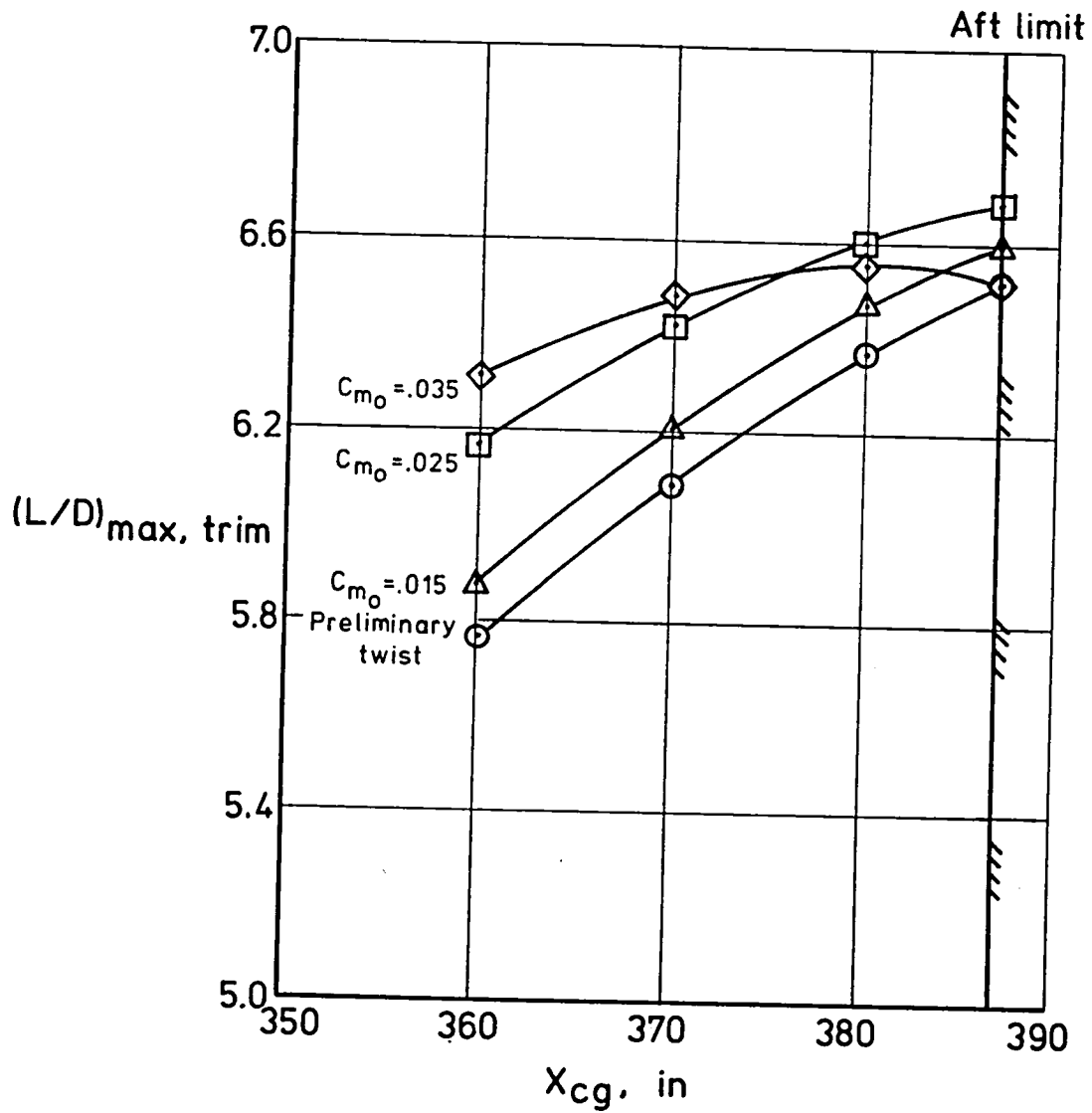
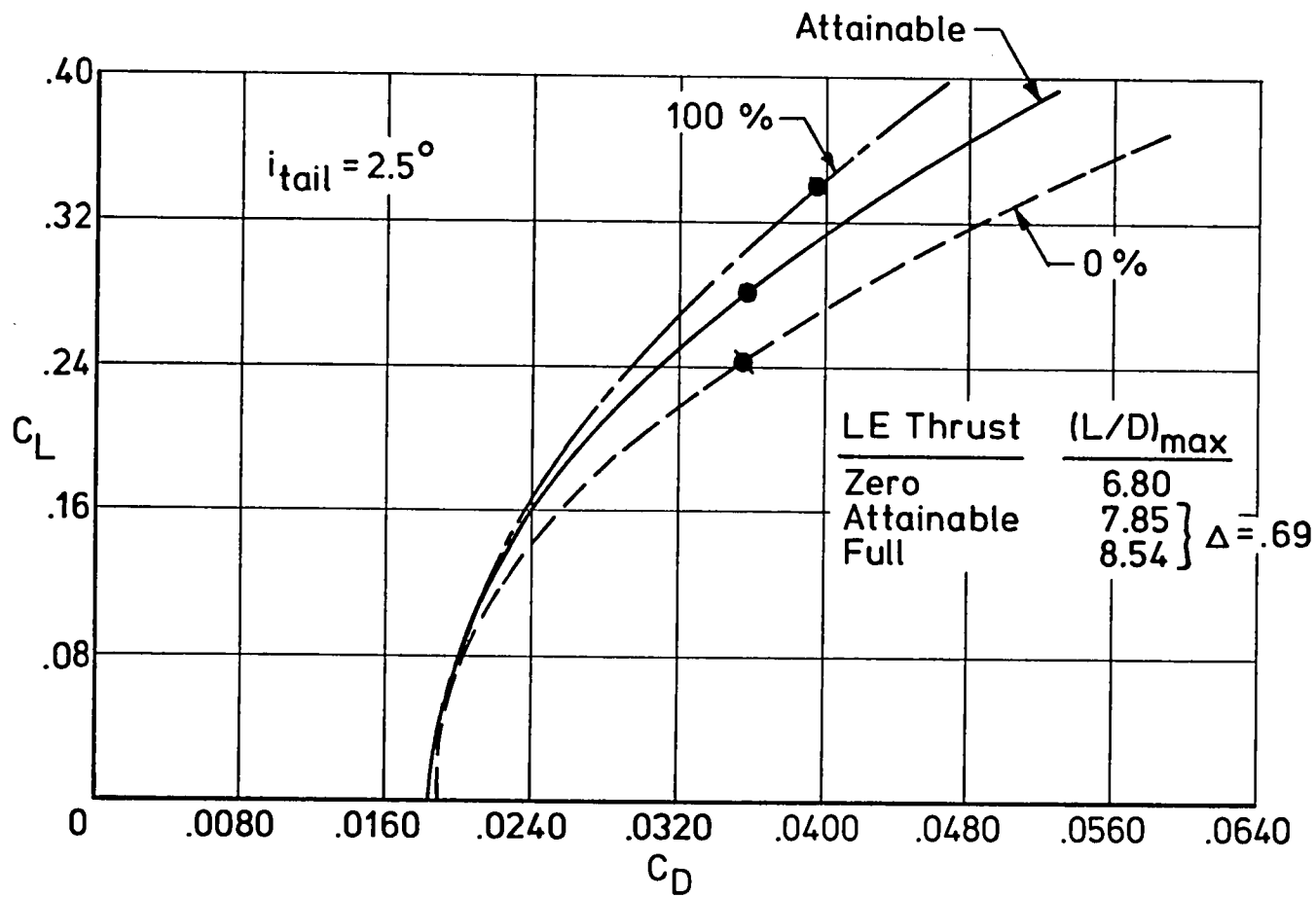Figure V-16. - Effect of C_{m_0} and center-of-gravity location on the trimmed $(L/D)_{MAX}$.
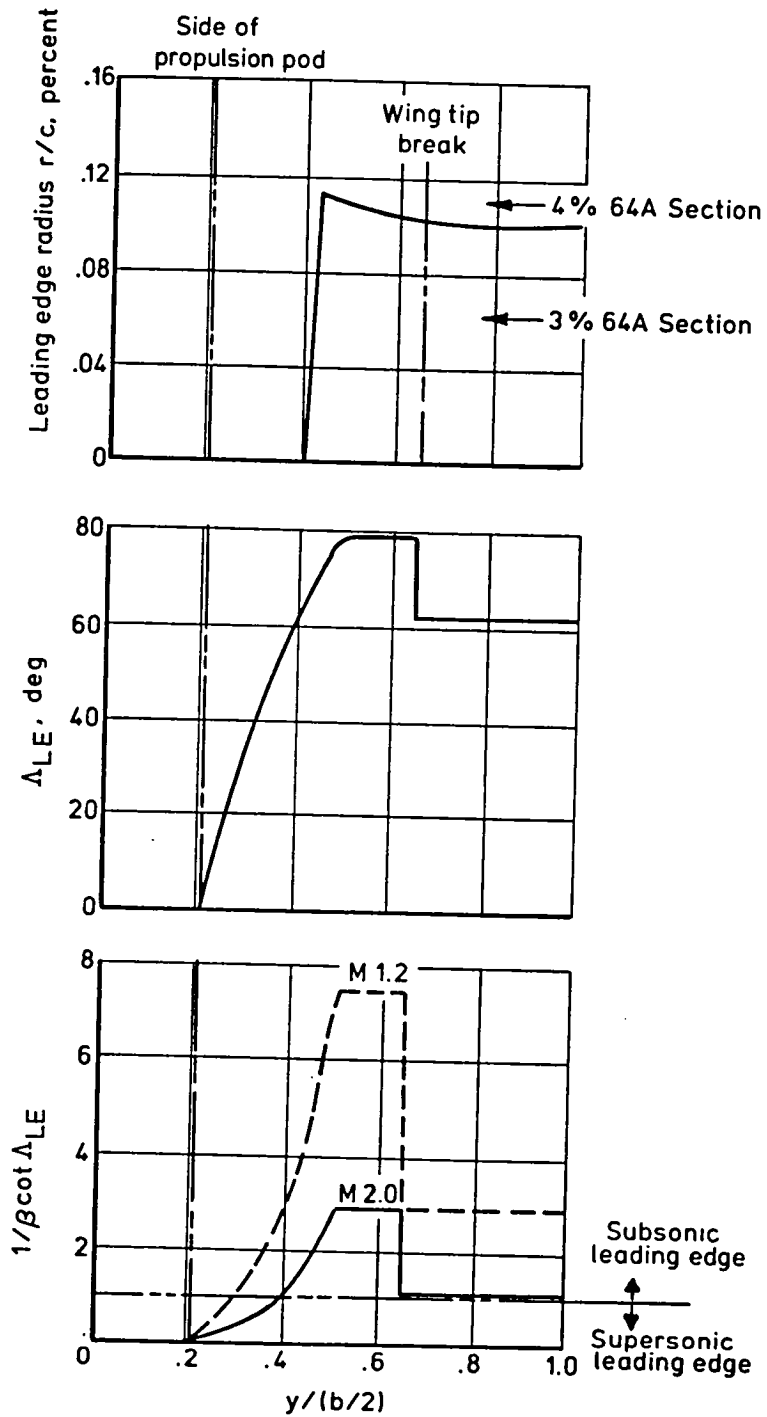
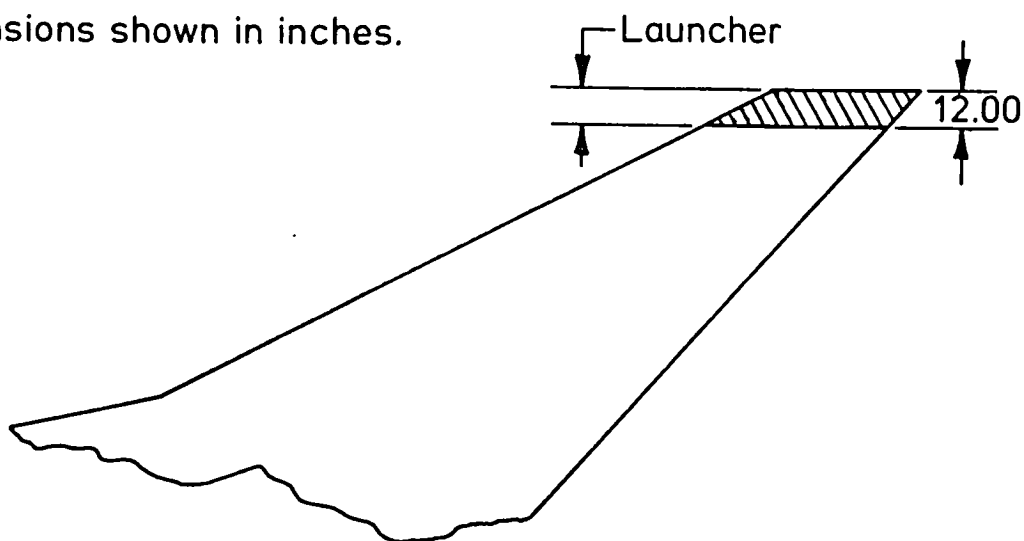Figure V-17. - Spanwise distribution of wing leading-edge sweep, radius, and thrust parameter.

Figure V-18. - Effect of leading-edge thrust on aerodynamic performance.
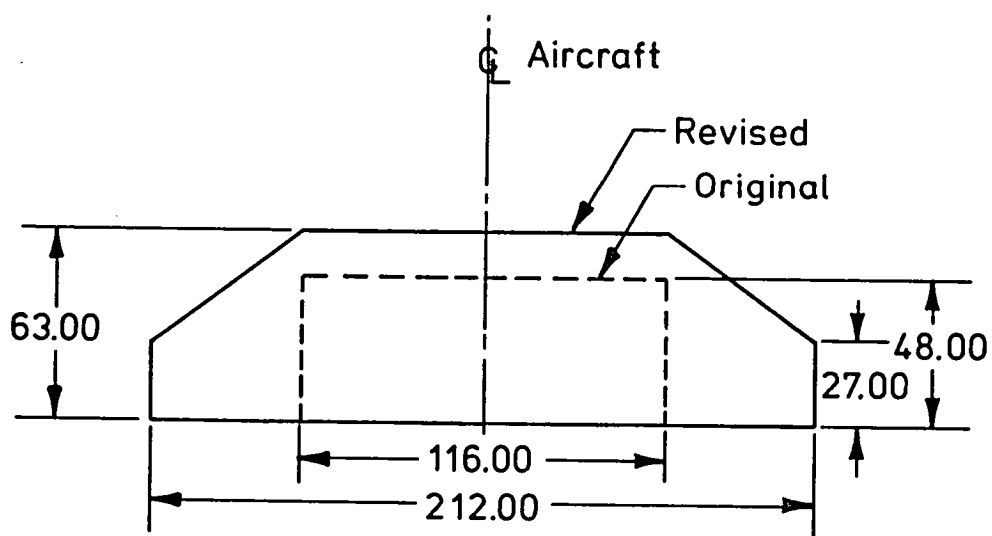
(b) Mach 1.2, 34 300 ft

Figure V-18. – Concluded.

Dimensions shown in inches.

(a) Representation of missile launcher.

(b) Revised horizontal tail geometry.

Figure V-19. - Incorporation of wing tip missile launcher and revisions to horizontal tail geometry for the baseline configuration.
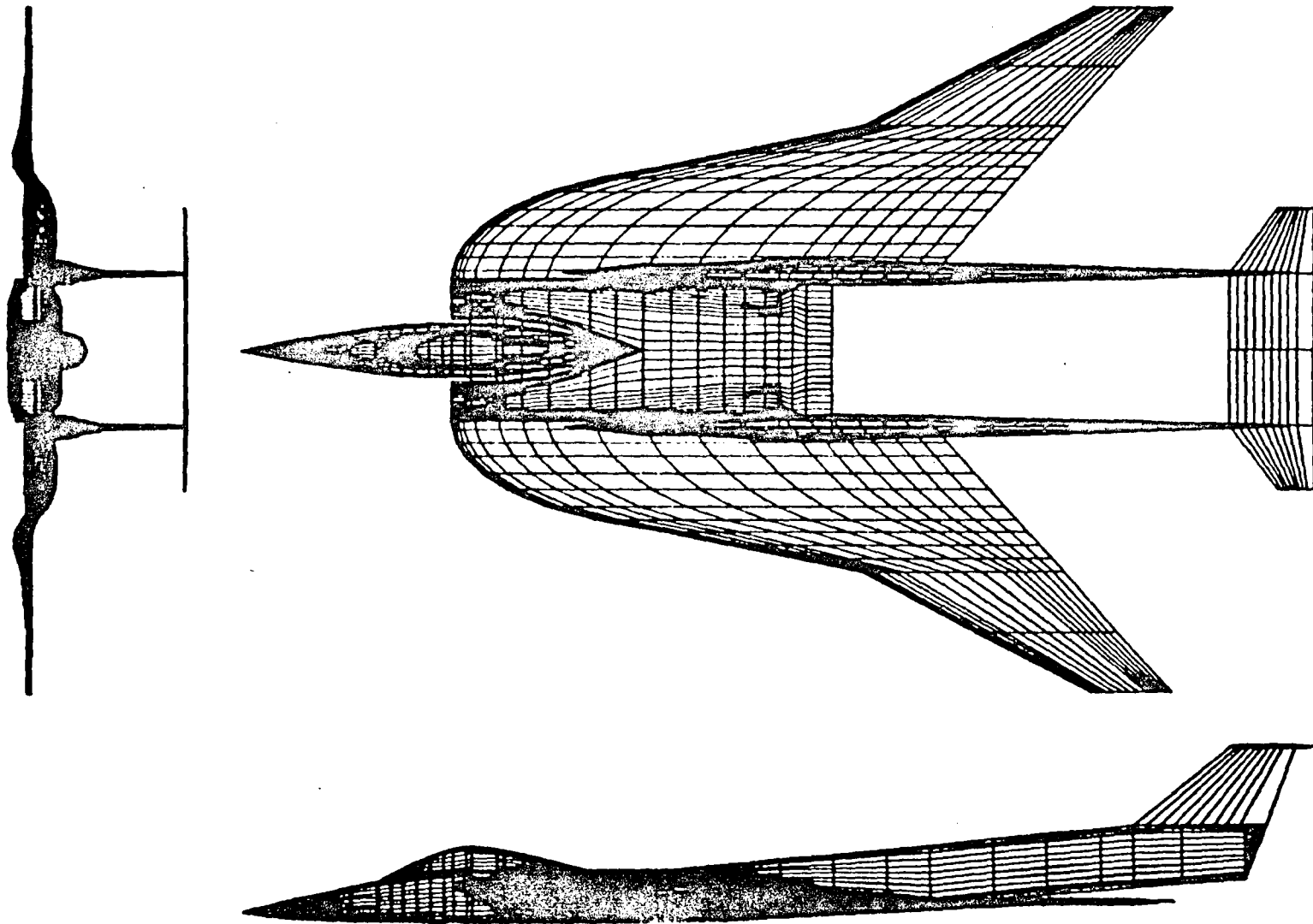
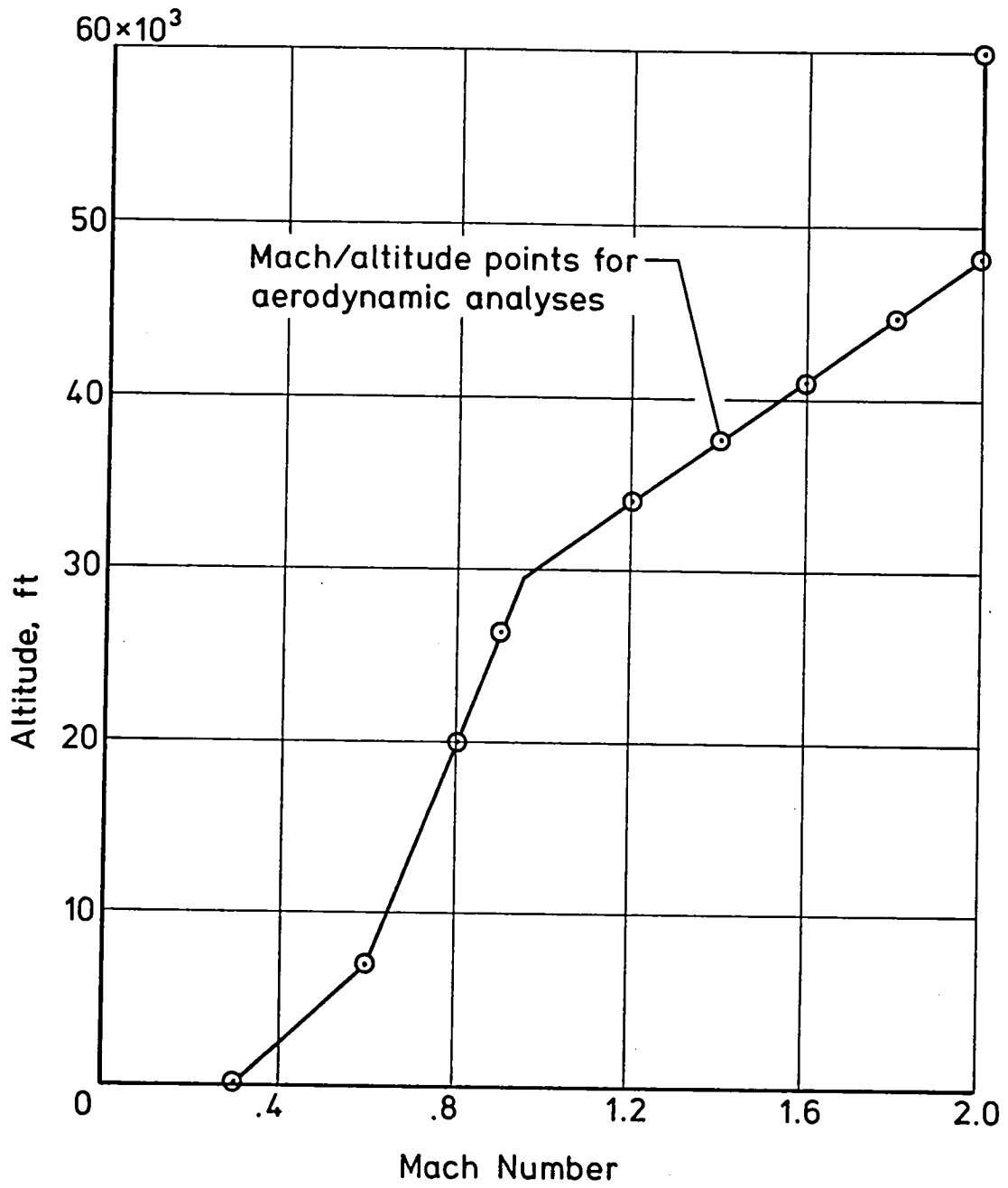Figure V-20. - The TBF-1 baseline configuration.

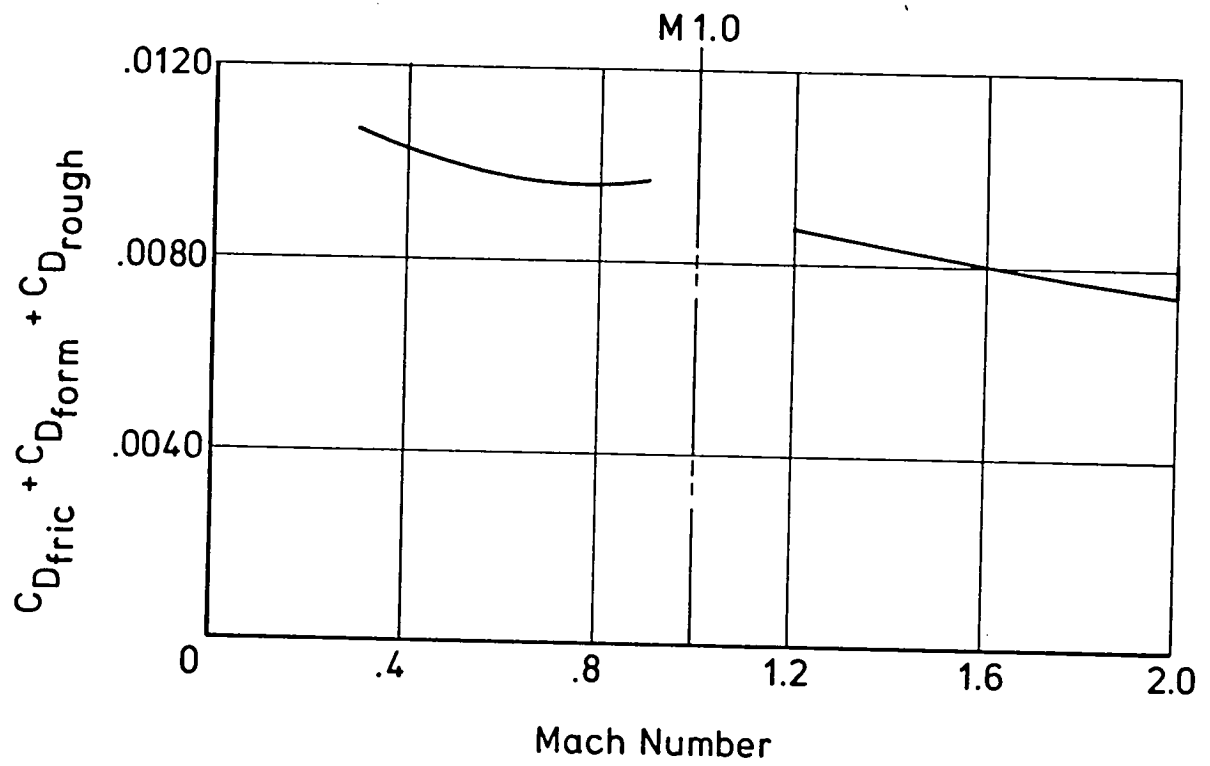Figure V-21. - Climb profile for aerodynamic analyses.

Figure V-22. - Variation of skin friction, form, and roughness drag with Mach number.
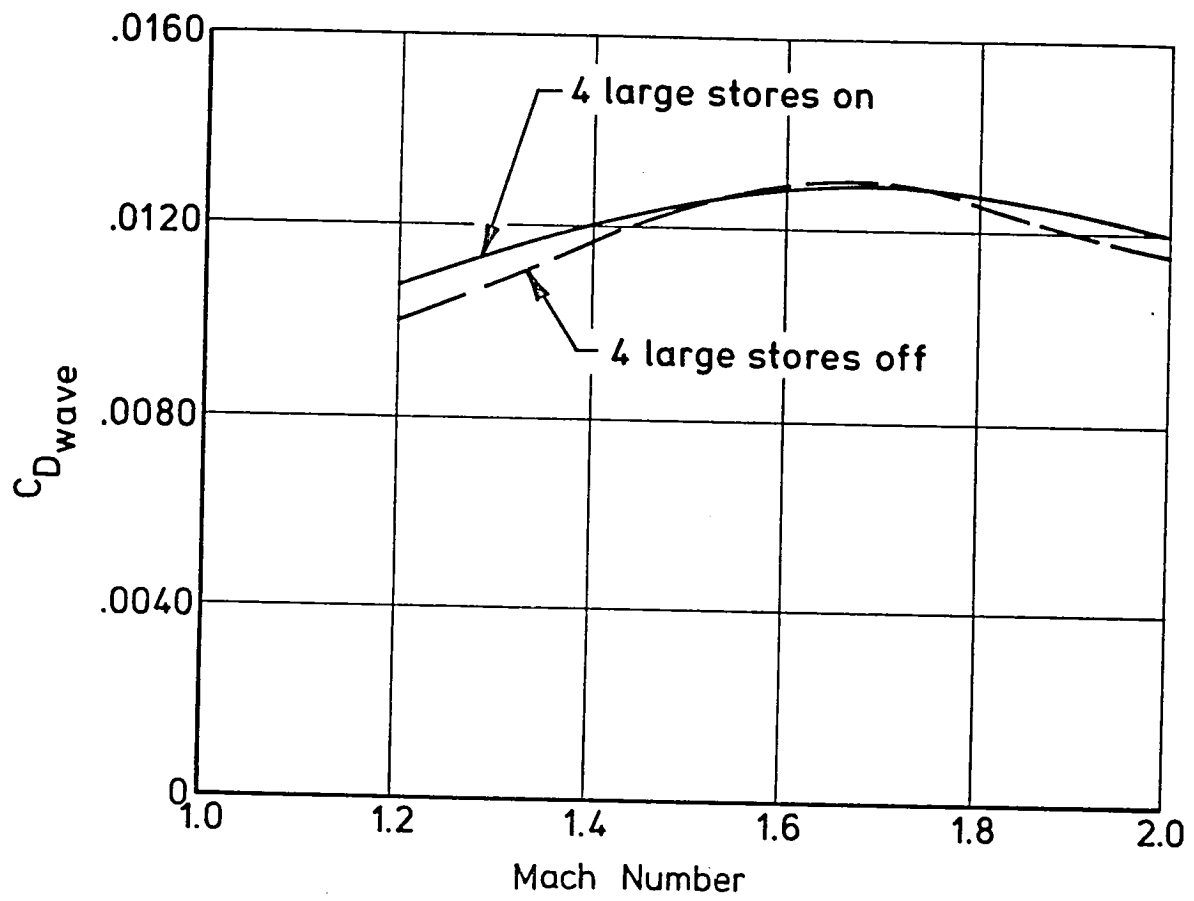
Figure V-23. - Zero-lift wave drag variation with Mach number.
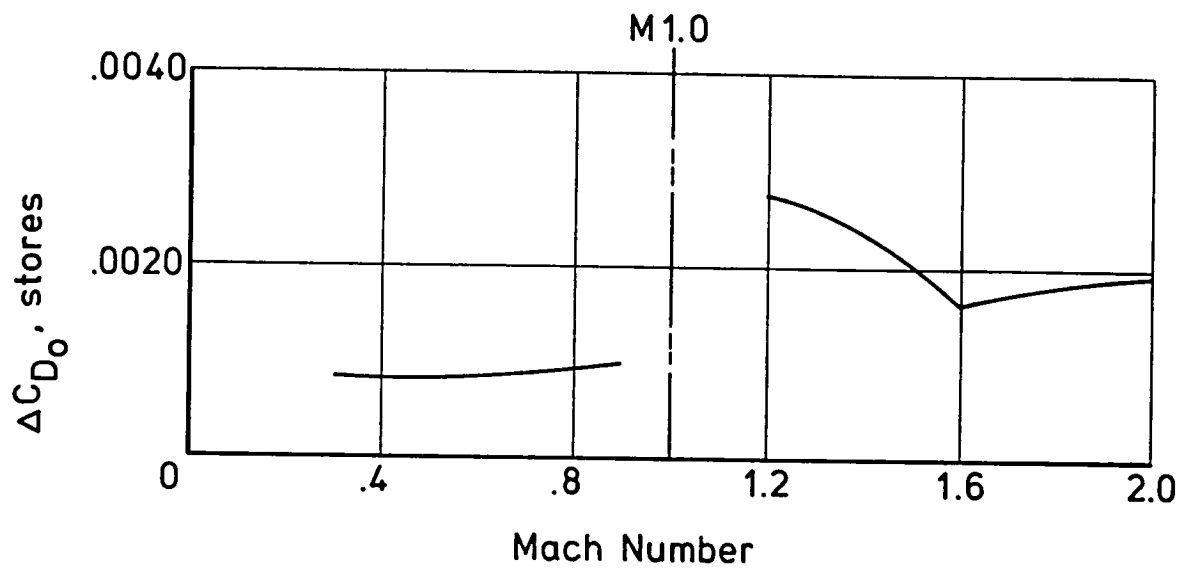
Figure V-24. - Zero-lift drag increment of the stores as a function of Mach number.
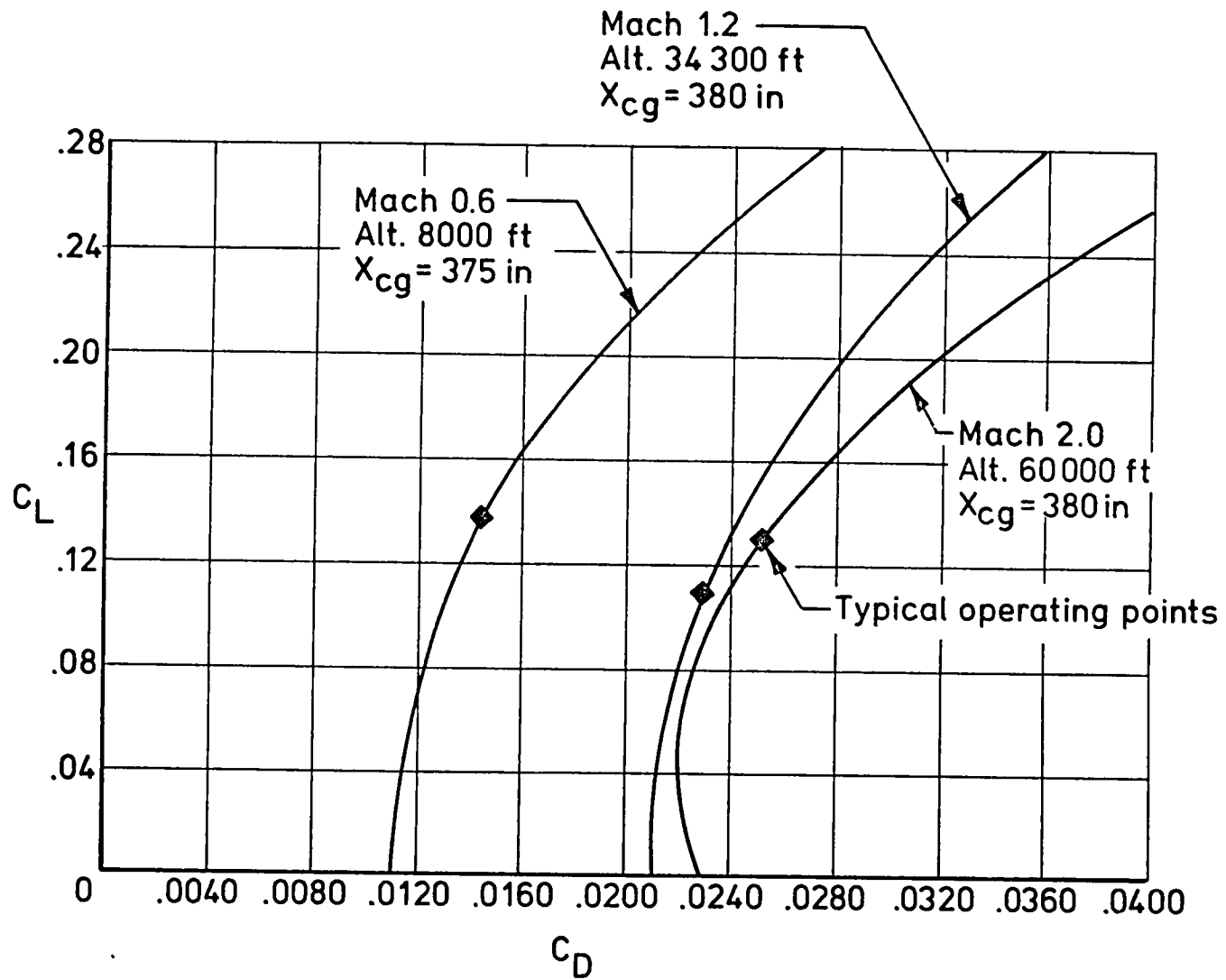
Figure V-25. - Typical trimmed polars.
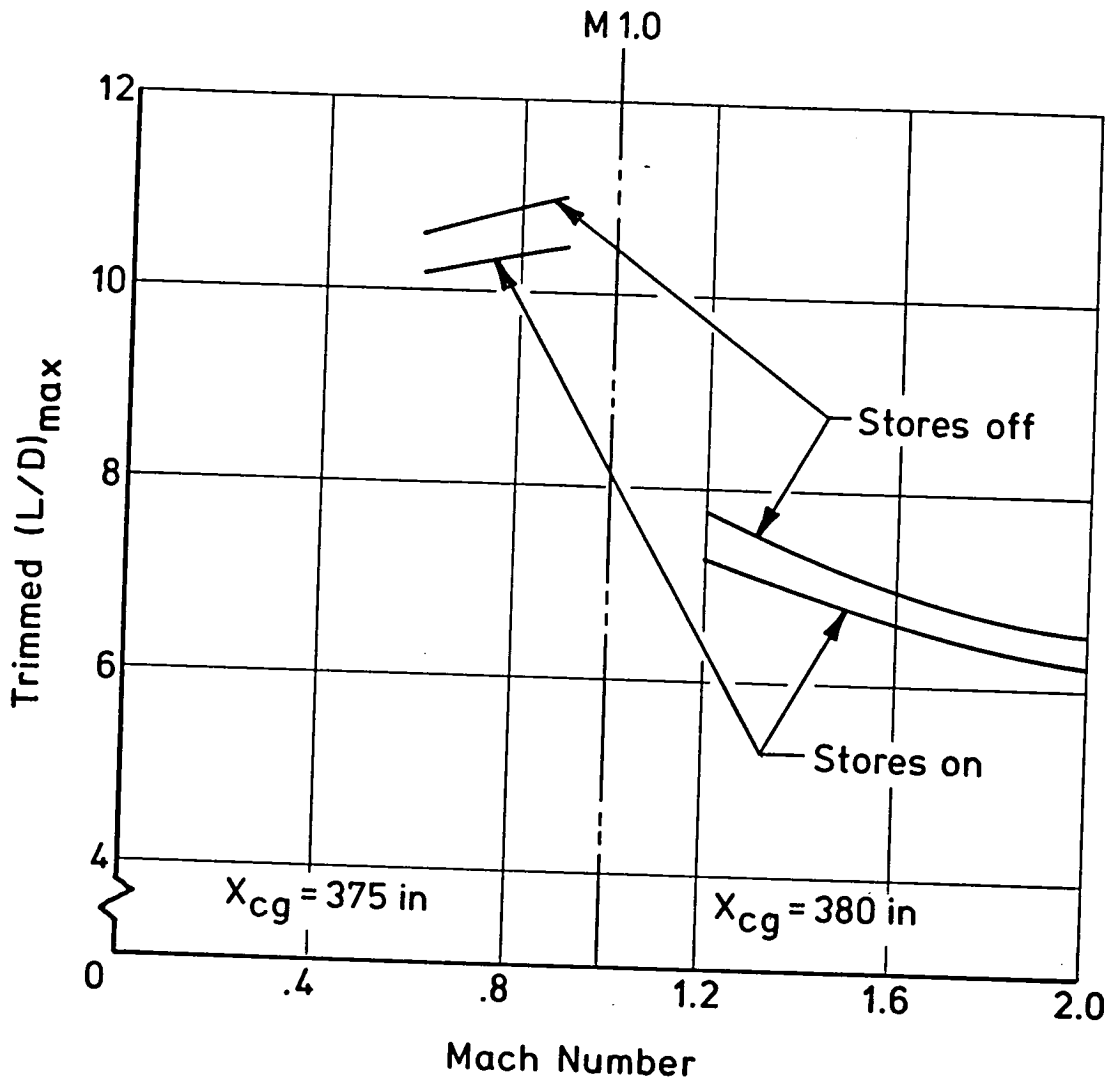
Figure V-26. - Trimmed $(L/D)_{MAX}$ variation with Mach number with stores on and off.

Flap	Area (ft^2)
L_1	9.585
T_1	19.793
T_2	15.366
T_3	15.976

Note:
Areas are for each side.
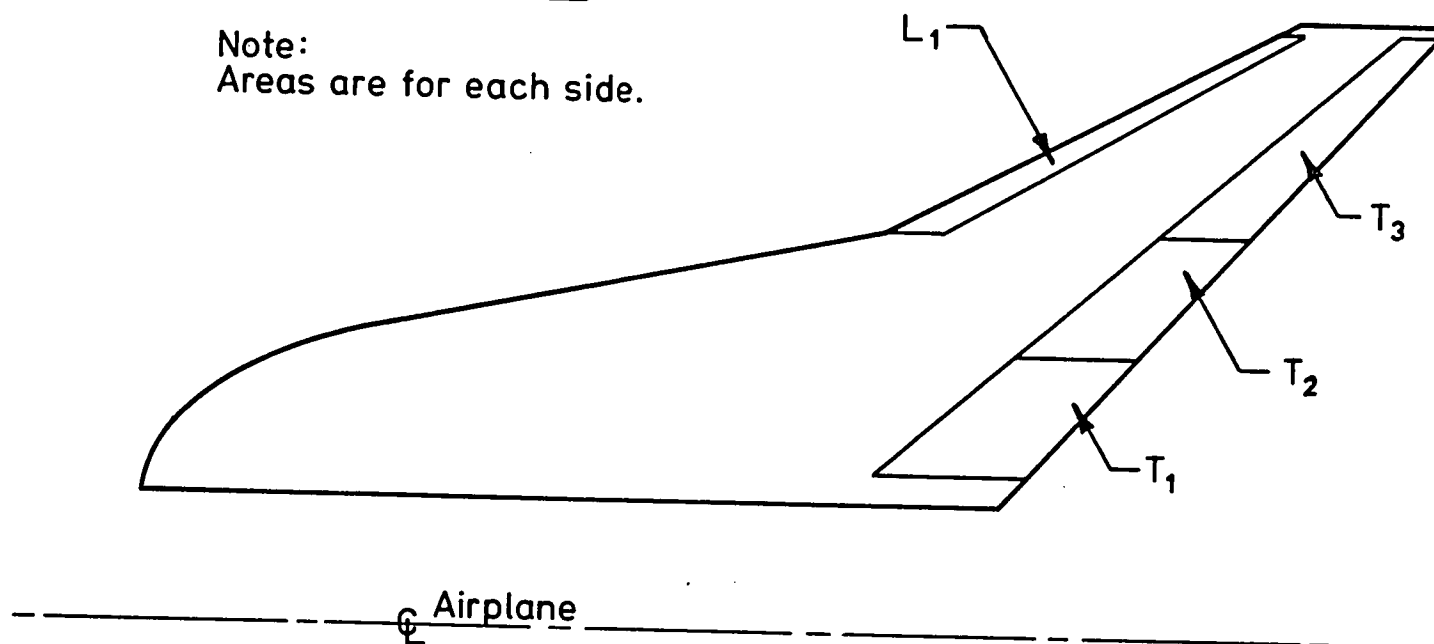
Figure V-27. — High-lift system.
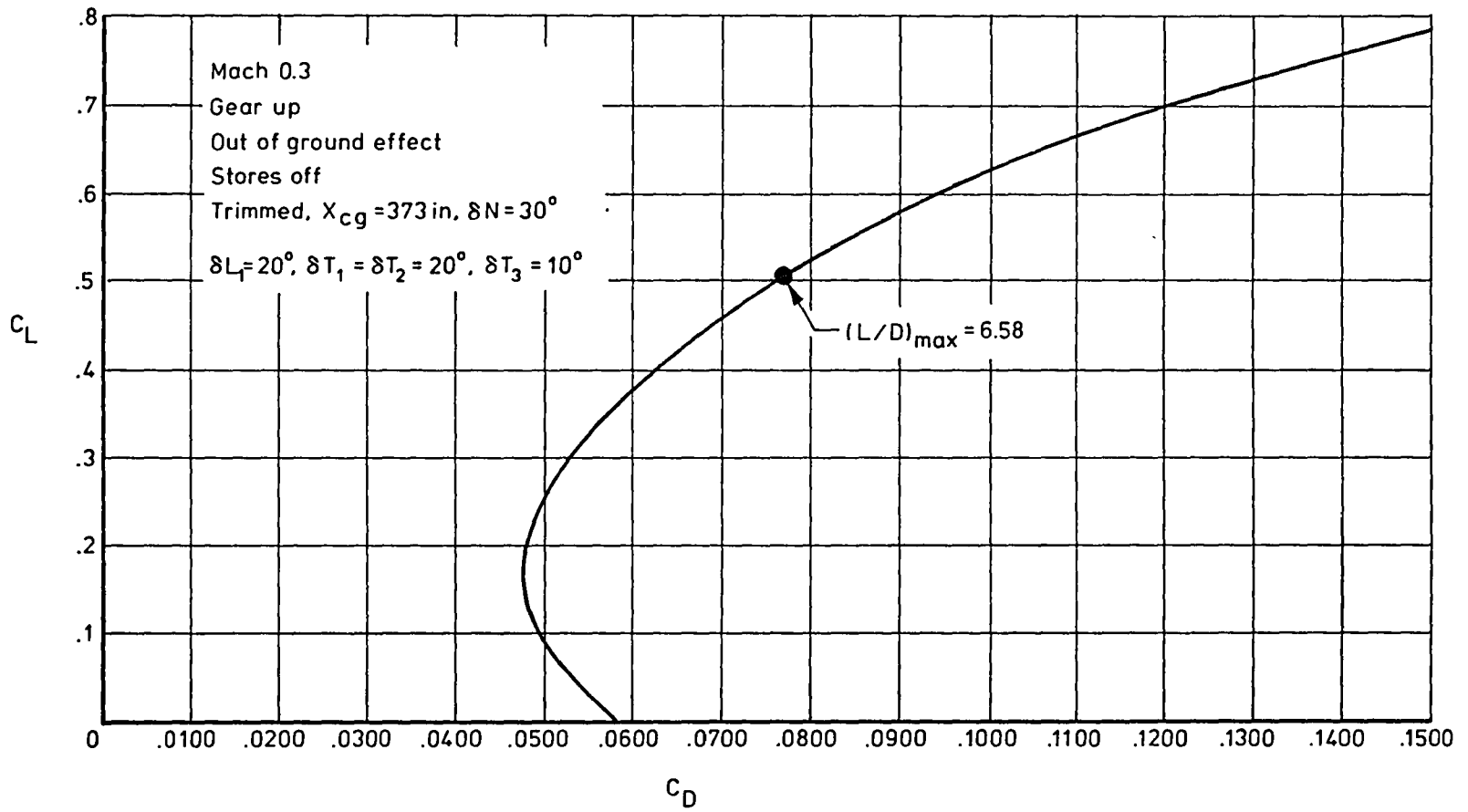
Figure V-28. - Low-speed drag polar.
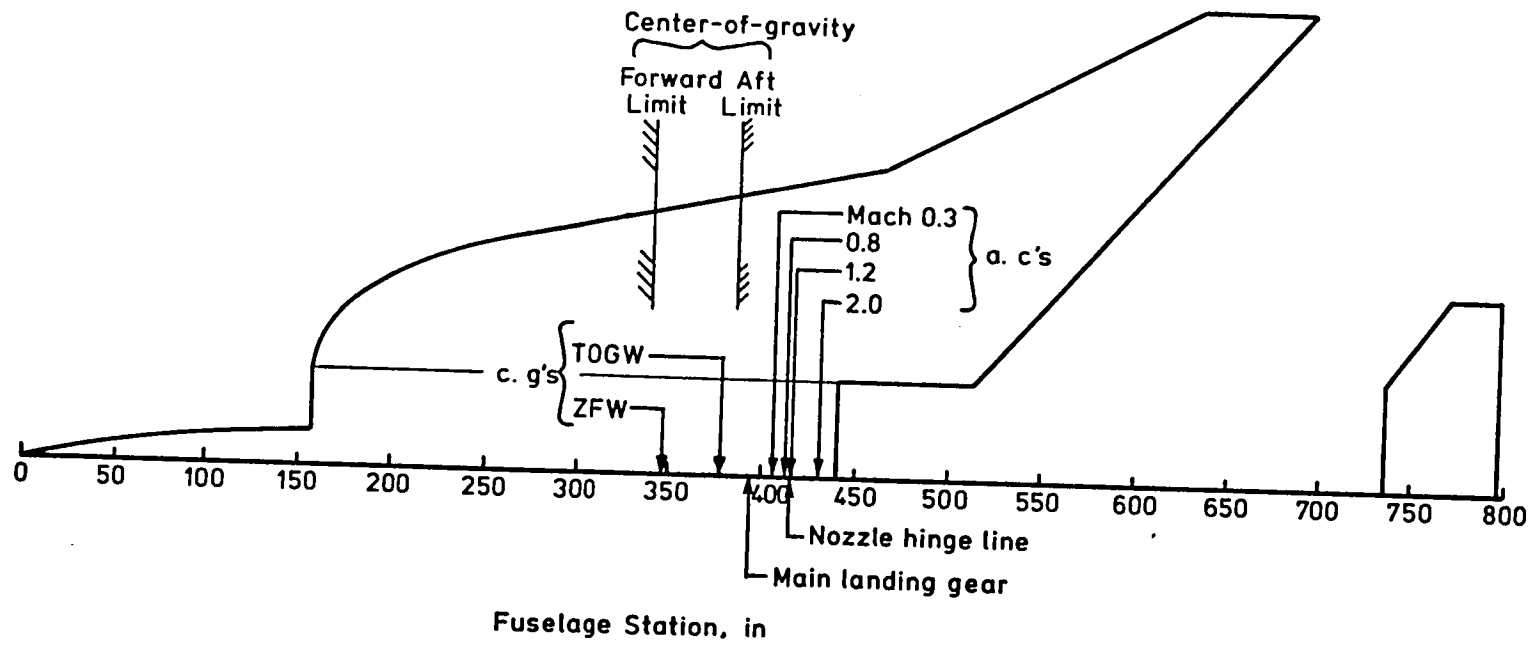
Figure V-29. - Aerodynamic centers and centers-of-gravity
for the baseline configuration.
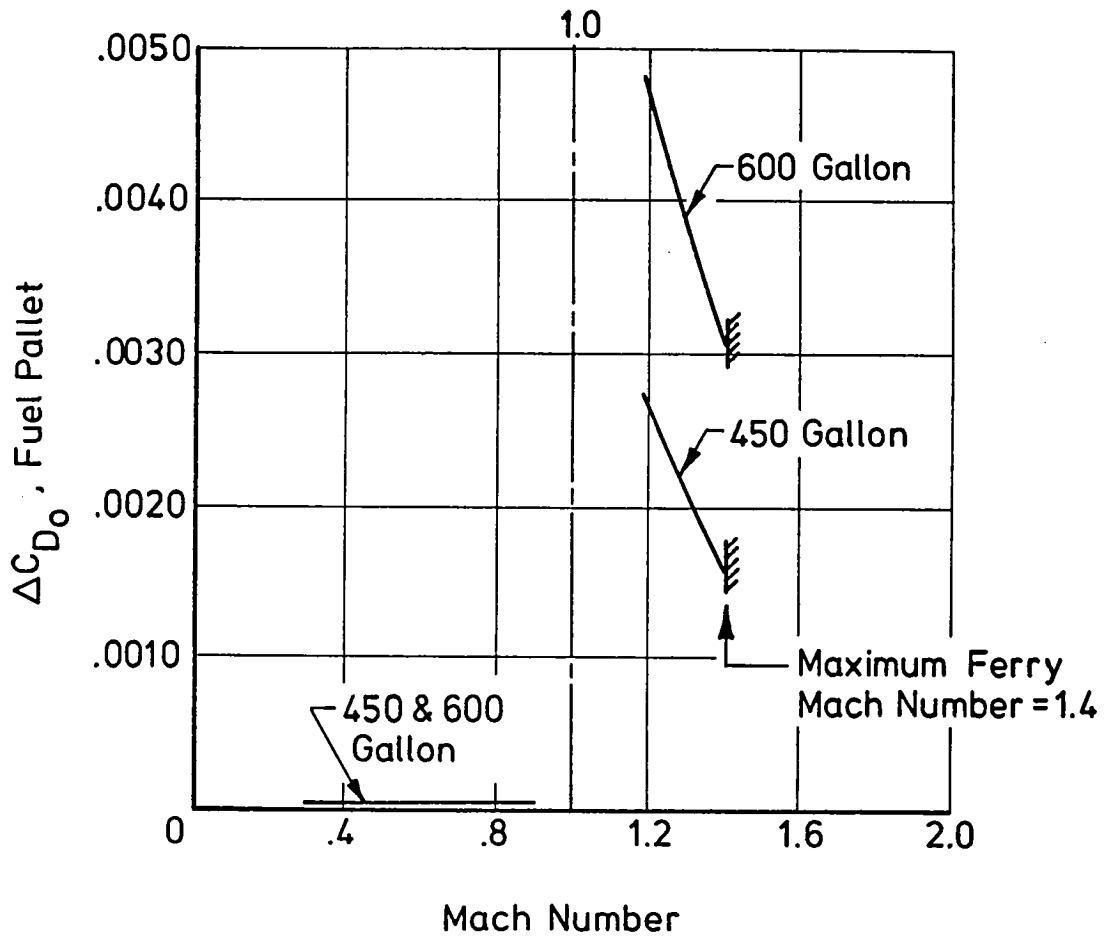
Figure V-30. - Zero-lift drag increment for fuel pallets.

Figure V-31. — Maneuver polar.

PART VI. - CONFIGURATION SIZING AND PERFORMANCE ANALYSIS

W. E. Foss, Jr.

Design Mission

The design mission for the present study is an all supersonic (Mach 2.0) profile with a radius of 500 nautical miles. The mission is conducted with internal fuel and includes a payload of 4,558 pounds which is expended at the combat radius station. The aircraft takeoff and landing ground roll must not exceed 1,000 feet, and the transonic acceleration and maneuver performance must be comparable with existing state-of-the-art fighter aircraft.
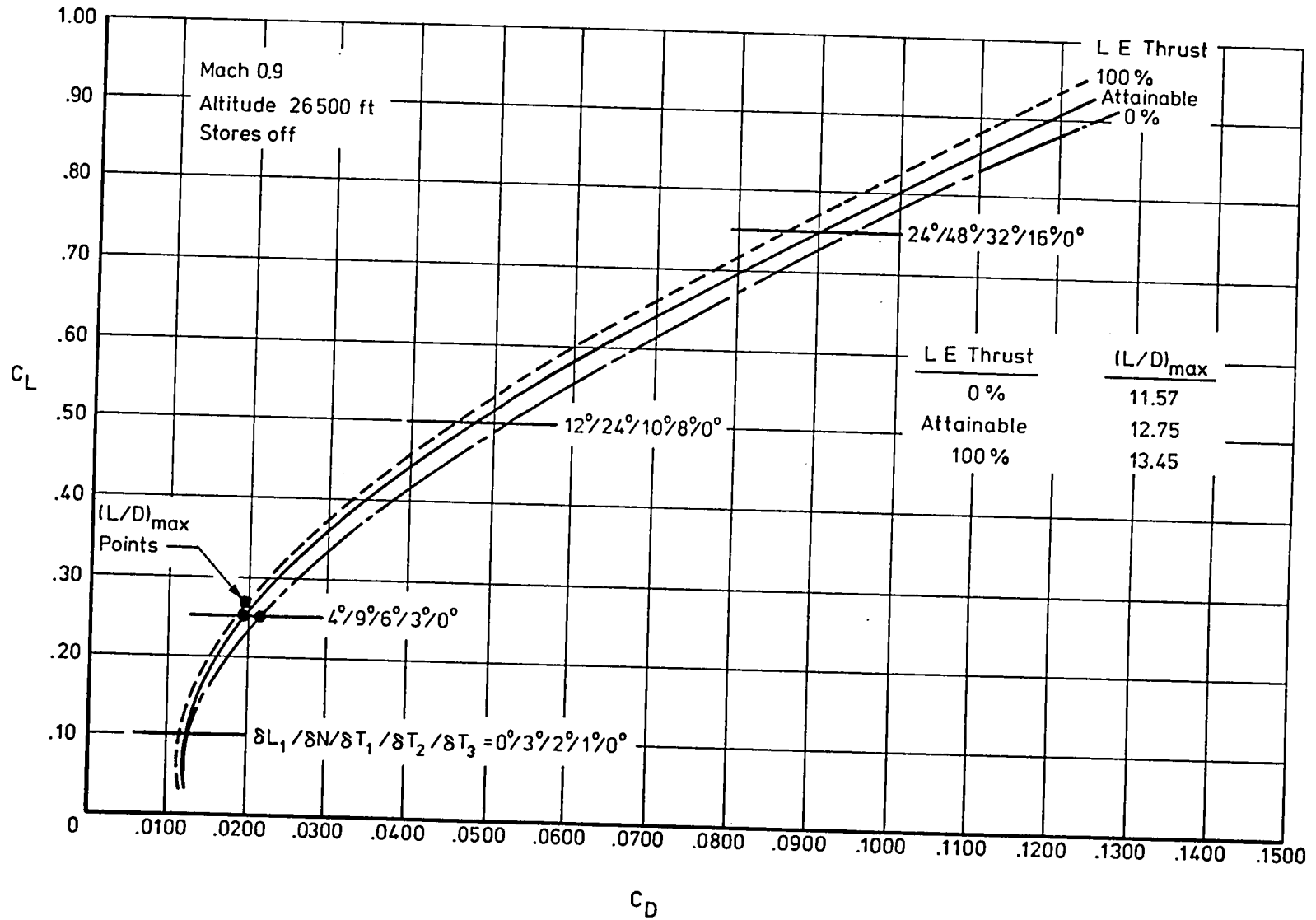
Specific mission ground rules and fuel allowances are as follows: The takeoff fuel allowance is the fuel required to operate the engines for one minute at the maximum augmented thrust level and then for two minutes at the maximum non-augmented thrust level. The climb and acceleration to the initial cruise condition is conducted at the maximum augmented thrust level along a Mach number-altitude profile typical of high performance aircraft (see figure V-21). All cruise segments are computed as a climbing cruise at constant lift coefficient, utilizing the Breguet cruise factor (V(L/D)/SFC), n.mi.) determined at the beginning of the segment. At the combat radius, the payload is dropped instantaneously with no effect on performance other than the associated drag and weight reductions. The combat fuel allowance consists of the fuel required for one and one-half turns at the maximum sustained turn rate for the cruise Mach number at an altitude of 40,000 feet. The sustained turn rate is calculated for a clean aircraft (no external stores) and for a combat weight equal to the aircraft operating weight empty (OWE) plus one-half of the internal fuel. The turn radius is included in the overall mission radius. On the return leg, the fuel and range increments to decelerate the aircraft from the cruise Mach number to a Mach number of 0.85 are included in the performance. An additional range increment of 10 nautical miles is credited to the return radius to account for the descent to sea level. The reserve fuel allowance is the fuel required to hold for 20 minutes at sea level.

The takeoff performance incorporates the following assumptions: At the start of the roll, the aircraft is at the ground-roll angle of attack (α = -2°) with the flaps and engine nozzle at zero degrees. The aircraft accelerates at maximum

thrust level until the velocity V_R to begin rotation is attained. This velocity is calculated by analysis of moment equilibrium at rotation. At V_R, the aircraft begins to rotate (4°/sec) and the flaps and the engine nozzle angle are changed to 30 degrees. The ground roll distance is the distance at which the aircraft beings to lift off. The takeoff distance, when quoted, is the distance required for the aircraft to clear a 50 foot obstacle.

The landing performance includes the following assumptions: The landing weight is assumed to be equal to the operating weight empty, plus the payload, plus five percent of the internal fuel. The nominal approach is along a 6-degree glide slope, with an angle of attack of 10°, and with both the flaps and the engine nozzle deflected 10°. A drag brake producing a drag coefficient of .0300 is deployed. During the final approach to touchdown, the velocity is assumed to decrease by 11 percent. At touchdown, the aircraft is assumed to be at the ground-roll angle of attack, with the flaps and nozzle deflection angle at zero degrees, and with engines operating at idle thrust. The aircraft accelerates down the runway for one second before wheel brakes are applied. Another one-half second time interval is required before the full braking coefficient (.35) is attained. Thrust reverser application begins one and one-half seconds after touchdown. A two-second time interval is assumed to activate the thrust reverser mechanism and to bring the engines up to full non-augmented power; thus, the thrust reversers are in full operation three and one-half seconds after touchdown. A thrust reversal effectiveness of 50 percent of the maximum non-augmented thrust has been assumed. No decay of the thrust reversers with decreasing aircraft velocity is assumed. The ground roll distance is the distance required to decelerate the aircraft from touchdown to a full stop.

The transonic acceleration capability of the aircraft is defined as the time in minutes required to accelerate from M = .70 to M = 1.80 at an altitude of 35,000 feet. The acceleration is calculated using the maximum augmented thrust level, for the aircraft including external stores, and for the combat weight previously defined. A time interval of 1.25 minutes is assumed to be the state-of-the-art performance level.

The maneuverability characteristics are determined for the maximum augmented thrust level, for a clean aircraft (no external stores), at combat weight for several Mach number and altitude conditions. Both the maximum instantaneous

specific power ((T-D) V/W)) and the maximum sustained load factor (and associated turn rate) are calculated. The sustained load factor requirement is 5.0 at M = 0.90 and 30,000 feet altitude and at M = 2.0 and 45,000 feet altitude.

Performance Analysis Method

Performance for the design mission and the operational items described above was calculated using a computer program documented in reference VI-1. The calculations utilize the U.S. Standard Atmosphere, 1962, and include the effects of thrust inclination and of gravity variation with altitude, of which the most significant is the thrust inclination. Inclination reduces the required aerodynamic lift at a given flight condition, and results in a lower level of drag, particularly at the high load factors considered in maneuverability calculations.

The capability of the referenced computer program has been expanded to permit the resizing of an input baseline aircraft design to determine combinations of takeoff gross weight, wing loading W/S, and thrust loading T/W which will attain the required radius for a given mission profile definition. In this mode, the aircraft gross weight, W/S and T/W are varied internally by the program to meet the mission radius requirements. The propulsion data are scaled to correspond to the desired engine size, and the operating weight empty is adjusted to reflect the configuration component weight changes. The aerodynamic lift and drag are natural functions of the desired wing area, but the basic aerodynamic coefficients are not modified to reflect the relative size changes between the wing and the other aircraft components. If the thrust-weight ratio and wing loading of the resized aircraft are far from those of the original baseline aircraft, the aerodynamic characteristics for a new baseline aircraft should be developed by configuration specialists and the performance verified.

Configuration Sizing and Performance

The baseline aircraft for the present concept has a wing loading of 69.4 psf, a thrust-weight ratio of 1.36, and a takeoff gross weight of 47,000 pounds. The resulting radius for the mission described above is 662 n.mi. This baseline concept was then resized for the design radius of 500 n.mi. and a complete performance analysis conducted. Figure VI-1 is a "Thumbprint Plot" which contains contours of constant aircraft takeoff gross weight on a grid of aircraft T/W and

W/S. All aircraft meet the design radius of 500 n.mi. Superimposed on the same grid are curves which represent specific operational constraints. All aircraft above the constraint curves meet the design mission radius and also meet or exceed the performance specifications of the operational constraints. The lowest takeoff gross weight that just meets the operational constraints would be about 38,500 pounds with a thrust-weight ratio of about 0.97 and a wing loading of approximately 64 psf. However, a higher T/W ratio is of interest for military aircraft to attain high levels of energy maneuverability and to maintain short takeoff performance on alternate missions with increased store loadings. Therefore, an aircraft with a thrust-weight ratio of 1.40, a wing loading of 70 psf, and with a takeoff gross weight of 42,750 pounds has been selected as the design-point aircraft. The takeoff ground roll distance, transonic acceleration time, and sustained load factors for this high thrust-weight ratio airplane are superior to the constraint values. For the 42,750 pound aircraft, the ground roll distances are 430 feet for takeoff and 1,000 feet for landing. The transonic acceleration time is .71 minutes. The sustained load factor is 7.0 at M = .90 and 30,000 feet altitude and is 6.8 at M = 2.0 and 45,000 feet altitude.

Effect of Advanced Engine Technology

The effect of advanced engine technology on takeoff gross weight is illustrated on figure VI-2. The data show the variation with aircraft thrust-weight ratio of the takeoff gross weight of the concept sized for a mission radius of 500 n.mi. The curves are for a wing loading of 70 psf and represent vertical cuts from the thumbprint plots. The lower curve was obtained from the data of figure VI-1 which utilized the advanced engine with an uninstalled engine thrust-weight ratio of about 10. The top curve was obtained from a thumbprint which utilized an engine with current state-of-art cycle performance characteristics and with an uninstalled engine thrust-weight ratio of about 8.0. The reduction in mission gross weight, when the advanced engine is used, varies from about 10,000 pounds at an aircraft T/W of .95 to about 20,000 pounds at a T/W of 1.4. The aircraft utilizing the engine with the higher thrust-weight ratio are of course less sensitive to increases in engine size. The middle curve was developed utilizing the advanced engine cycle performance characteristics but assuming that the engine thrust-weight ratio was the same as for the T/W = 8.0 engine. This curve indicates that about 75 percent of the overall reduction in mission gross

weight is due to the better cycle performance of the advanced engine and that only 25 percent of the reduction is accountable to the higher engine specific thrust.

Effect of Increased Thrust-Weight Ratio

Some of the beneficial effects of increased aircraft thrust-weight are shown in figures VI-3 and VI-4. Takeoff ground roll and sustained load factor at M = 0.90 and 30,000 feet are presented in figure VI-3. The takeoff roll is reduced to 430 feet for the aircraft with thrust-weight ratio = 1.4. For the same aircraft the sustained load factor, with the wing leading edge and trailing edge flaps set to optimum positions for maneuvering, is 7.0. With the flaps set for cruising flight, the sustained load factor is about 5.1. The sustained load factors are calculated for a thrust deflection angle of 10 degrees, which results in the best performance for these flight conditions. Figure VI-4 presents the energy maneuverability characteristics at three Mach number and altitude combinations for two thrust-weight ratios. The calculations assumed maximum augmented thrust with a thrust deflection angle of 10 degrees and with the aircraft at combat weight in the clean configuration (no external stores). The favorable effect of the higher thrust-weight ratio is apparent at all flight conditions in terms of the increase in the maximum instantaneous specific power (at a load factor of 1.0) and in the increase in the maximum sustained load factor (for zero specific power). A load factor of 7.0 can be sustained at M = 0.9 and at M = 1.6, and a load factor of 6.8 can be sustained at M = 2.0.

Current operational fighter aircraft can sustain a load factor of about 4.0 at a Mach number of 0.9 and an altitude of 30,000 feet, and about 3.0 at M = 1.6 and 40,000 feet. For these aircraft, sustained flight at M = 2.0 and 45,000 feet generally is not possible. Both the aircraft concepts represented on figure VI-4, and in particular the concept with the higher thrust-weight, have superior maneuver performance to current fighters. The degree to which the Mach number and altitude "combat arena" has been expanded with respect to that of a current transonic fighter aircraft is shown in figure VI-5. The figure presents, on an altitude versus Mach number grid, the sustained load factor (n) contours for the concept with a thrust-weight 1.4. The curve on the lower right portion of the figure represents the operating limit line for the aircraft and engine (assumed to be a dynamic pressure of 1,800 psf). The shaded area represents the operating envelope of a current fighter aircraft for a sustained load factor of 4.0, and the cross-

hatched area is the comparable envelope for the present concept. The sustained 4g combat arena is about 2 1/2 times larger for the present concept.

Ferry Mission Capability

The long range cruise performance of a fighter aircraft is of importance for logistic operations. The range capability of the aircraft concept was calculated for a ferry mission profile for several cruise Mach numbers. For these missions, the cruise calculations utilize an average of the Brequet factors determined at the beginning and end of each segment. For the missions with a cruise Mach number of 0.90, the climb and acceleration to the cruise conditions utilized maximum non-augmented thrust and the takeoff fuel allowance does not include any operations at maximum augmented thrust level. The wing tip missiles are carried throughout the mission. The long range missiles are not carried and are replaced with two different types of external fuel tanks. The first type is the same size as the long range missiles and is carried in a semi-submerged position in the store cavity, as indicated in figure II-6. The ferry mission range is calculated utilizing these tanks, which are retained throughout the mission, at cruise Mach numbers of 0.90, 1.40, and 2.00. The second type of tank is a conformal fuel pallet which also fits into the area normally occupied by the large missiles. These units are designed to provide a low-drag installation for Mach numbers up to 1.4. Figure II-7 illustrates the pallet geometry, and the zero-lift drag increments associated with these units are presented in figure V-30. Each of these units, when resized for the base-point aircraft wing area of 610 square feet, contains 512 gallons (3,330 pounds) of fuel and is assumed to have an empty weight of 250 pounds. These tanks are also retained throughout the mission and ferry mission performance is calculated for cruise Mach numbers of 0.90 and 1.40.

Table VI-I presents the range capability for the ferry mission profile with the external fuel tanks previously defined. With the store cavity tanks and a full internal fuel load the takeoff gross weight is 44,797 pounds. The range for cruise Mach numbers of 0.90, 1.40, and 2.0 are 2,923, 2,259, and 2,121 nautical miles respectively, with corresponding mission times of 5.7, 2.8, and 1.9 hours. With the conformal fuel pallets and a full internal fuel load the takeoff gross weight is 49,116 pounds. The range for cruise Mach numbers of 0.90 and 1.4 are 3,390 and 2,571 nautical miles respectively, with mission times of 6.6 and 3.2 hours. The

concept, therefore, has the capability of unrefueled intercontinental ferry missions.

REFERENCES

VI-1.   Foss, Willard E., Jr.: A Computer Technique for Detailed Analysis of Mission Radius and Manuverability Characteristics of Fighter Aircraft. NASA TP 1837, 1981.

TABLE VI-I. – LONG RANGE FERRY MISSION PERFORMANCE OF THE CONCEPT SIZED FOR 500 n.mi. DESIGN MISSION WITH A T/W = 1.4. TIP MISSILES AND TANKS ARE RETAINED.

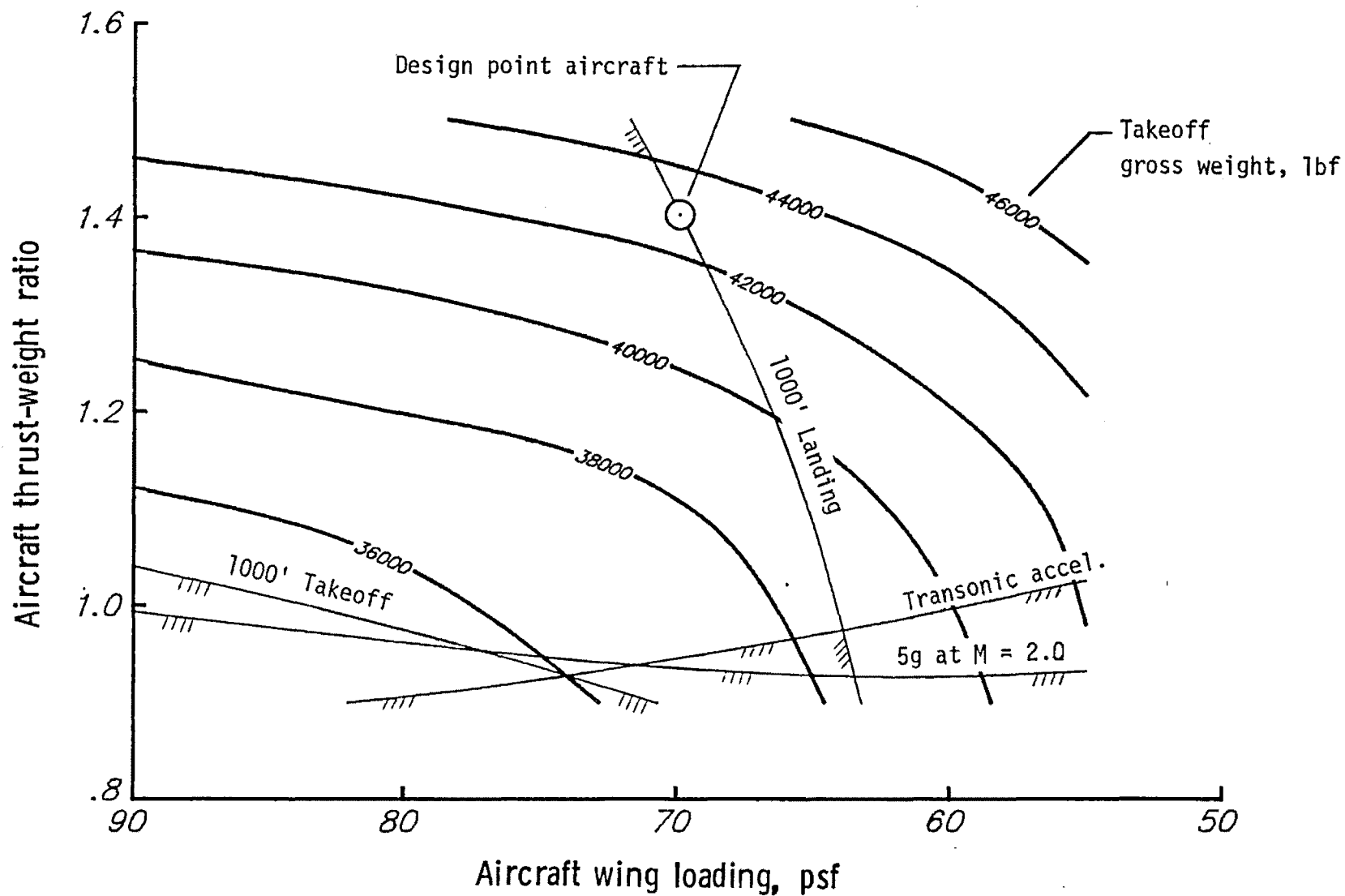| EXTERNAL TANKS	STORE CAVITY			CONFORMAL PALLET	
GROSS WEIGHT, lbf	44,797			49,116	
CRUISE MACH NUMBER	0.9	1.4	2.0	0.9	1.4
RANGE, n.mi.	2,923	2,259	2,121	3,390	2,571
TIME, hrs	5.7	2.8	1.9	6.6	3.2

Figure VI-1. – Effect of wing loading and thrust-weight ratio on the takeoff gross weight of the concept, when sized for the design mission radius of 500 nautical miles at a cruise Mach = 2.0.
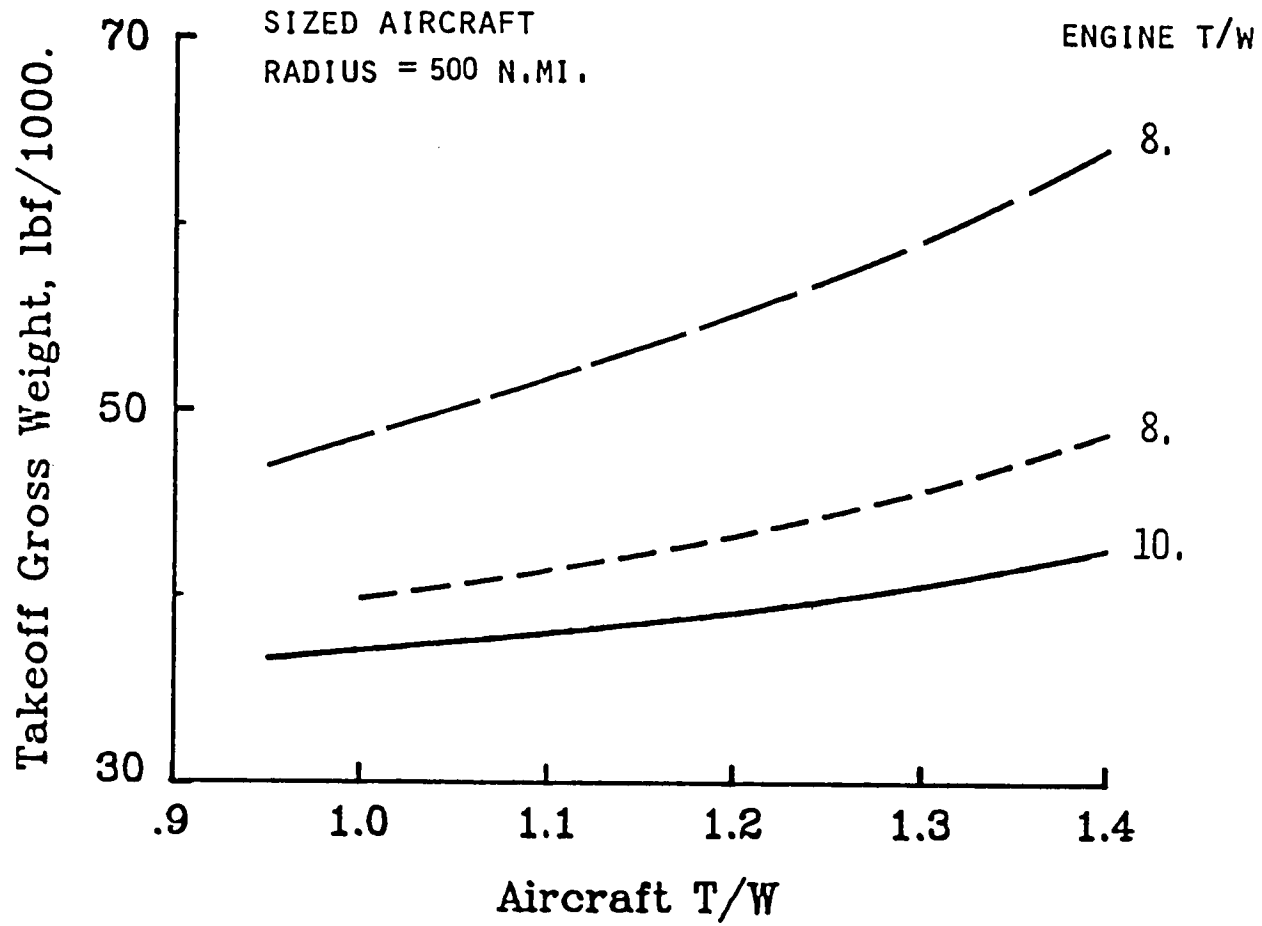
Figure VI-2. – Effect of advanced engine technology on the takeoff gross weight as a function of aircraft thrust-weight ratio. Wing loading 70 psf.
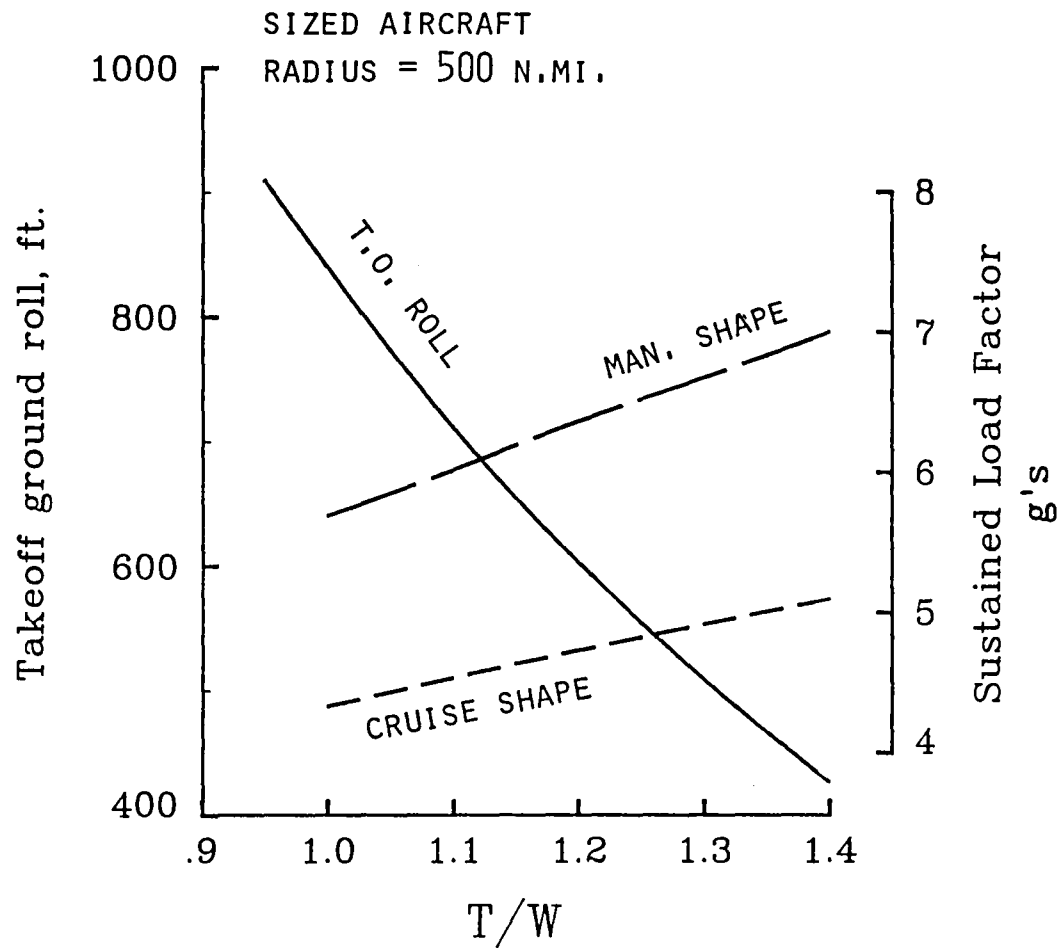
Figure VI-3. — Effect of thrust-weight ratio on the takeoff ground roll distance and on the sustained load factor capability at a Mach = 0.90 and an altitude of 30,000 feet.

T/W

— —○— — 1.00

——□—— 1.40

M=0.9
ALT=30000 FT

M=1.6
ALT=40000 FT

M=2.0
ALT=45000 FT

Specific Power ft/sec

1600

1200

800

400

0

-400

Load Factor , g's

1   3   5   7

Figure VI-4. - Energy maneuverability characteristics for two aircraft, sized
for the design mission with a wing loading of 70 psf.

MAXIMUM THRUST
CLEAN CONFIGURATION

Figure VI-5. – Contours of sustained load factor for the design point aircraft.

CONCLUDING REMARKS

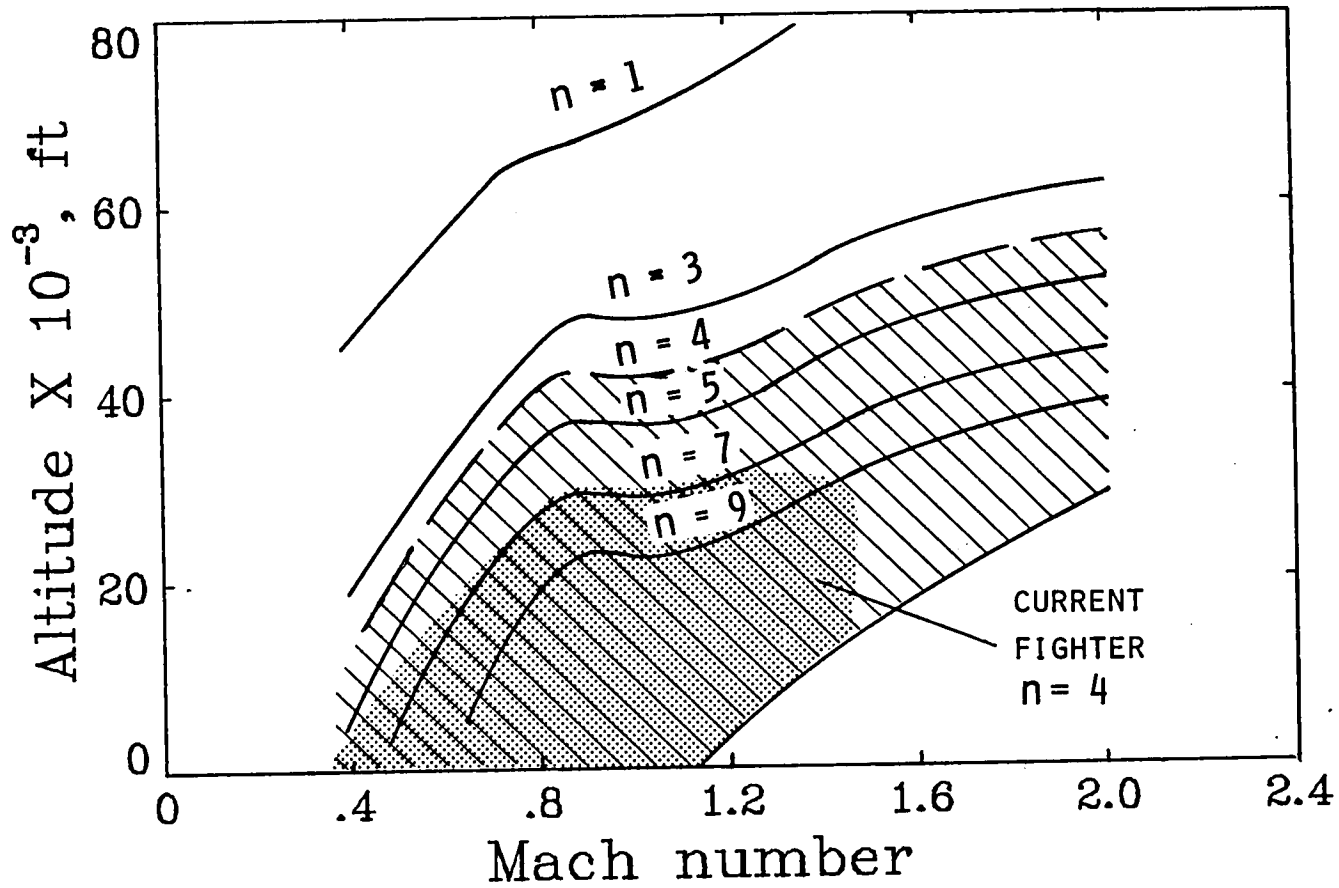The application of advanced and emerging technologies to a fighter aircraft concept configured for short field operation has been discussed. The concept referred to as the twin-boom fighter (TBF-1) relies on a two-dimensional vectoring/reversing nozzle to provide STOL performance while also achieving efficient long range supersonic cruise. A key feature is that the propulsion package is placed so that the nozzle hinge line is near the aircraft center-of-gravity to allow large vector angles and, thus, provide large values of direct lift while minimizing thrust-induced moments which must be trimmed aerodynamically. Utilizing an advanced military engine (1985 state-of-the-art) with an uninstalled engine thrust-to-weight ratio of 10, an overall thrust to takeoff-gross-weight ratio of 1.4 resulted with relatively small penalty in the takeoff-gross-weight of the concept. As indicated in the Performance Analysis section, the increased performance for a fighter associated with the increased aircraft thrust-weight ratio was considered an appropriate trade for the weight increase. In addition to large improvements in takeoff and maneuver performance, thrust-weight ratios this much greater than 1.0 offer the potential for vertical operation on both takeoff and landing if a suitable control system and acceptable handling qualities can be developed.

Other advanced technologies used are superplastic formed/diffusion bonded (SPF/DB) titanium structure for all primary aircraft structure; advanced avionics/controls through the use of an advanced control system, cockpit displays, and sensors; supersonic wing design; and conformal weapons carriage. The integration of these advanced technologies resulted in an aircraft concept that had a takeoff gross weight of approximately 43,000 pounds with 4,558 pounds payload capable of a 500 nautical mile radius of action at Mach 2.0 cruise. Sustained maneuver load factors considerably in excess of current fighter aircraft could be achieved over an expanded flight envelope. Takeoff and landing ground-roll distances less than the 1,000-feet goal could easily be achieved using thrust vectoring only after rotation on takeoff and during approach for landing. A better understanding of low-speed control and handling qualities could permit a more aggressive use of thrust vectoring to achieve even better takeoff and landing performance. Further, the performance analysis indicated an unrefueled intercontinental ferry range by using conformal fuel pallets which fit into the area normally occupied by missiles.

In summary, the integration of a limited number of advanced technologies into an advanced fighter concept indicate that large gains in takeoff and landing performance, maneuver, acceleration, and supersonic cruise can be achieved.

1. Report No. NASA TM-85777	2. Government Accession No.	3. Recipient's Catalog No.
4. Title and Subtitle DEVELOPMENT AND ANALYSIS OF A STOL SUPERSONIC CRUISE FIGHTER CONCEPT		5. Report Date MARCH 1984
		6. Performing Organization Code 505-43-43-01
7. Author(s) S. M. Dollyhigh, W. E. Foss, Jr. and S. J. Morris, Jr. K. B. Walkley, E. E. Swanson, and A. W. Robins		8. Performing Organization Report No.
		10. Work Unit No.
9. Performing Organization Name and Address NASA Langley Research Center Hampton, VA 23665		
		11. Contract or Grant No.
12. Sponsoring Agency Name and Address National Aeronautics and Space Administration Washington, DC 20546		13. Type of Report and Period Covered Technical Memorandum
		14. Sponsoring Agency Code

15. Supplementary Notes

S. M. Dollyhigh, W. E. Foss, Jr., and S. J. Morris, Jr. - NASA Langley Research Center
K. B. Walkley, E. E. Swanson, and A. W. Robins - Kentron International, Inc.,
  Hampton, Virginia

16. Abstract

The application of advanced and emerging technologies to a fighter aircraft concept is presented. The concept, which is referred to as the twin-boom fighter (TBF-1), relies on a two-dimensional vectoring/reversing nozzle to provide STOL performance while also achieving efficient long range supersonic cruise. A key feature is that the propulsion package is placed so that the nozzle hinge line is near the aircraft center-of-gravity to allow large vector angles and, thus, provide large values of direct lift while minimizing the moments to be trimmed. The configuration name is derived from the long twin booms extending aft of the engine to the twin vertical tails which have a single horizontal tail mounted atop and between them. Advanced technologies utilized were an advanced engine (1985 state-of-the-art), superplastic formed/diffusion bonded titanium structure, advanced controls/avionics/displays, supersonic wing design, and conformal weapons carriage. The integration of advanced technologies into this concept indicate that large gains in takeoff and landing performance, maneuver, acceleration, supersonic cruise speed, and range can be achieved relative to current fighter concepts.

17. Key Words (Suggested by Author(s)) Supersonic Fighter STOL Aircraft Optimization	18. Distribution Statement Unclassified - Unlimited Star Category 05 - Aircraft Design, Testing and Performance
19. Security Classif. (of this report) UNCLASSIFIED	20. Security Classif. (of this page) UNCLASSIFIED	21. No. of Pages 85	22. Price A05